Benzodioxane-benzamides as promising inhibitors of Escherichia coli FtsZ

Lorenzo Suigo, Begoña Monterroso, Marta Sobrinos-Sanguino, Carlos Alfonso, Valentina Straniero, Germán Rivas, Silvia Zorrilla, Ermanno Valoti, William Margolin

PII: S0141-8130(23)03294-4

DOI: https://doi.org/10.1016/j.ijbiomac.2023.126398

Reference: BIOMAC 126398

To appear in: *International Journal of Biological Macromolecules*

Received date: 23 May 2023

Revised date: 2 August 2023

Accepted date: 16 August 2023

Please cite this article as: L. Suigo, B. Monterroso, M. Sobrinos-Sanguino, et al., Benzodioxane-benzamides as promising inhibitors of Escherichia coli FtsZ, *International Journal of Biological Macromolecules* (2023), https://doi.org/10.1016/j.ijbiomac.2023.126398

Benzodioxane-benzamides as promising inhibitors of *Escherichia coli* FtsZ

Lorenzo Suigo [a], Begoña Monterroso [b,†], Marta Sobrinos-Sanguino [b,†], Carlos Alfonso [b], Valentina Straniero [a], Germán Rivas [b], Silvia Zorrilla [b,*], Ermanno Valoti [a,*], William Margolin [c,*]

[a] Dipartimento di Scienze Farmaceutiche, Università degli Studi di Milano, Via Luigi Mangiagalli, 25, 20133 Milano, Italy. lorenzo.suigo@unimi.it (L.S.), valentina.straniero@unimi.it (V.S.), ermanno.valoti@unimi.it (E.V.)

[b] Centro de Investigaciones Biológicas Margarita Salas, Consejo Superior de Investigaciones Científicas (CSIC), 28040 Madrid, Spain. monterroso@cib.csic.es (B.M.), marta.sobrinos@cib.csic.es (M.S.-S.), carlosa@cib.csic.es (C.A.) grivas@cib.csic.es (G.R.), silvia@cib.csic.es (S.Z.)

[c] Department of Microbiology and Molecular Genetics, McGovern Medical School, University of Texas, Houston, 77030 Texas, USA. William.Margolin@uth.tmc.edu (W.M.)

[†] These authors contributed equally to this work

Abstract

The conserved process of cell division in bacteria has been a long-standing target for antimicrobials, although there are few examples of potent broad-spectrum compounds that inhibit this process. Most currently available compounds acting on division are directed towards the FtsZ protein, a self-assembling GTPase that is a central element of the division machinery in most bacteria. Benzodioxane-benzamides are promising candidates, but poorly explored in Gram-negatives. We have tested a number of these compounds on *E. coli* FtsZ and found that many of them significantly stabilized the polymers against disassembly and reduced the GTPase activity. Reconstitution in crowded cell-like conditions showed that FtsZ bundles were also susceptible to these compounds, including some compounds that were inactive on protofilaments in dilute conditions. They efficiently killed *E. coli* cells defective in the AcrAB efflux pump. The activity of the compounds on cell growth and division generally showed a good correlation with their effect *in vitro*, and our experiments are consistent with FtsZ being the target *in vivo*. Our results uncover the detrimental effects of benzodioxane-benzamides on permeable *E. coli* cells *via* its central division protein, implying that lead compounds may be found within this class for the development of antibiotics against Gram-negative bacteria.

Keywords: Antimicrobial resistance, Bacterial division, FtsZ assembly, Gram-negative bacteria, 1,4-Benzodioxane-benzamides, *in vitro* and *in vivo*.

1. Introduction

In modern medicine, the problem of antibiotic resistance is of utmost importance for public health. According to the World Health Organization (WHO), even if the awareness regarding this threat is increasing over time, the number of antibacterial agents in clinical development is well below the global requirements to overcome this worrying issue [1]. In 2017, the WHO published the first list of antibiotic-resistant "priority pathogens", which is a catalogue of 12 bacterial families, further divided into three categories, according to the urgency of need for new antibiotics: critical, high and medium priority [2]. It is noteworthy that the majority of these listed bacterial strains are Gram-negative pathogens.

As a result, developing agents capable of interacting with new molecular targets is a crucial and urgent need. Cell division continues to hold great promise among the essential bacterial processes unexploited as targets for potential antimicrobials used in therapy. Indeed, FtsZ, the central organizing protein of the division machinery (the divisome) is highly conserved among most bacterial species and significantly differs from its human structural homologue, tubulin [3]. In preparation for cell division, FtsZ assembles early to form a Z-

ring at the centre of the cell, using GTP to polymerize. The Z-ring provides a scaffold on which the remaining division proteins assemble due to their ability to interact directly or indirectly with FtsZ [4]. The fully assembled divisome contains a septal peptidoglycan synthesising complex and is connected to other periplasmic and outer membrane proteins [5,6]. The activities present in the divisome build a septum that ultimately splits the cells in two almost equal halves. Given the central role of FtsZ in this essential process, the overall interest of the scientific community in this protein as a potential target for antibiotics has increased in the last decades [3,7–10].

The capability of FtsZ to exist as oligomers or polymers in a nucleotide-dependent manner is crucial for its role in the context of the bacterial cell division process. Indeed, as extensively described in literature, GTP binds to FtsZ in a pocket that is highly conserved among all bacterial species, triggering its polymerization [4,11,12]. The site of GTP hydrolysis is formed at the interface between two units of FtsZ, and hydrolysis leads to FtsZ disassembly [4]. *In vitro*, FtsZ polymers are polymorphic, with their size and arrangement largely dependent on the solution conditions [13]. The basic FtsZ polymer is a single stranded protofilament, which is mainly observed in most dilute solution conditions near neutral pH [12,13]. In the presence of crowding agents that reproduce the cell interior, FtsZ forms bundles involving lateral interactions between protofilaments, and these bundles disassemble more slowly than single protofilaments [12,14,15].

Given the key role of GTP binding and hydrolysis for FtsZ function, molecules targeting this binding site have been synthesised and evaluated as potential antimicrobials [8,16]. However FtsZ harbours another druggable pocket, the interdomain cleft (IDC), which is located between the N-terminal and the C-terminal subdomains of the globular domain and involves the T7 loop that inserts into the adjacent monomer to activate GTPase activity [3,4,7,9]. Compared to the nucleotide binding site, there is more variability in the features of the IDC across bacterial species, including the overall size of the cavity and the nature of the residues [7]. Because this pocket is absent in tubulin, unlike the nucleotide binding site, it is the one targeted by most of the FtsZ inhibitors available to circumvent cytotoxicity [7].

Several FtsZ inhibitors are now known and they belong to different structural classes. Among them, the benzamide family and its reference compound PC190723, a 2,6-difluoro-3-substituted benzamide, have been widely studied [3,7,8], and the Structure-Activity Relationship (SAR) exploration culminated with the development of TXA707 and its prodrug TXA709, which is currently in Phase-1 clinical trials [7,17]. These compounds target the IDC [7] generally leading to the formation of foci containing FtsZ *in vivo* and reducing the GTPase activity *in vitro* [8,18,19]. Most of the benzamide derivatives display potent activity only against Gram-positive bacteria such as *Staphylococcus aureus* and *Bacillus subtilis,* while failing to inhibit growth of Gram negatives, likely due to the protective action of efflux pumps or the outer membrane permeability barrier [3]. The effects of PC190723 on *E. coli* cells and on FtsZ from this organism remain controversial [20–22]. The few reports of FtsZ inhibitors capable of targeting Gram-negative strains underscore the key roles of efflux pumps in these species and the need to genetically or chemically inhibit them to permit small molecule compounds to inhibit growth [17,21,23–25]. Specifically, two derivatives belonging to a benzamide class functionalized at the alkoxy fragment, TXA6101 and TXY6129, have shown inhibitory effects on *E. coli* FtsZ polymerization/bundling and morphological changes on efflux pump deficient *E. coli* that are consistent with FtsZ inhibition [17].

Over the last decade, we designed and developed a novel class of FtsZ inhibitors (hereafter named as FZXX): the 1,4-benzodioxane benzamides. This class originated by substituting the pyridothiazole moiety of PC190723 with a simpler 1,4-benzodioxane, a widely known scaffold in medicinal chemistry [26] whose synthesis and pharmacokinetic properties have been extensively investigated, leading to the development of FZ14 (Fig. 1) [27]. This compound, which possesses a slight anti-staphylococcal activity (MIC = 5 µg/ml *vs*

both Methicillin-sensitive and Methicillin-resistant *S. aureus*) represented the foundation for the development of this class.

Starting from FZ14, SAR analysis was conducted by modifying different portions of the lead compound (Fig. 1). Initially, the role of the positions 6- and 7- of the 1,4-benzodioxane ring was investigated. By analogy to PC190723, one chlorine atom was inserted in one or both positions, with better results obtained for the 7-substituted derivative. Indeed, this compound showed 10-fold increased antimicrobial activity versus both Methicillin-sensitive and Methicillin-resistant *S. aureus* compared to FZ14 [27]. Subsequently, substitution in the same position with a methyl ester resulted in FZ38, which has good antimicrobial properties [28]. Starting from this preliminary SAR analysis, the next step was to substitute the methyl ester group, which is chemically labile *in vivo*, with more stable ester bioisosters such as 1,2,4-oxadiazoles, leading to FZ82, FZ90 and others [23]. Parallel antimicrobial activity studies shed light on how the substitution of both the oxygens of the benzodioxane scaffold, and in particular of oxygen in position 1, is always detrimental [24,28]. Then, we developed and validated a computational model that revealed a narrow and lipophilic cleft within the IDC of *S. aureus* FtsZ that could be exploited to achieve additional interactions [23,24]. This led to compounds such as FZ94 and FZ101, characterized by the presence of a 1,4-naphthodioxane or a 5,6,7,8-tetrahydro-1,4-naphthodioxane ring, that display strong activity [29]. Lastly, using valuable insights gained with the aforementioned computational model, we investigated the impact of the linker length on the activities, as the *in-silico* model predicts two carbon atoms in the linker, instead of one, should enhance the potency [23,29]. As a result of this in-depth study of the SAR, we obtained compound FZ88 and two derivatives, FZ95 and FZ100 (Fig. 1**,** bottom), which represent the best modifications of these in-parallel evaluations, showing sub-micromolar activities towards both Methicillin-sensitive and Methicillin-resistant *S. aureus* [29]. To increase the polarity of FZ100, we also designed and synthesised one FZ100-hydroxylated derivative. Since we introduced an additional stereogenic centre, we isolated both diastereoisomers: *erythro* (FZ116) and *threo* (FZ117) (Fig. 2) [30]. Besides enhancing the overall polarity of the molecule, the additional -OH group within these molecules could be further exploited for the design of prodrugs, to tune their physical-chemical properties, or to couple fluorescent dyes, with diverse applications.

Despite the increases in potency of the benzodioxane-benzamide class of compounds towards Gram-positive bacteria, they had no activity on wild type Gram-negative bacteria such as *E. coli* ATCC 25922. In contrast, *E. coli* N43, a specific mutant lacking the AcrAB efflux system known to play a major role in antibiotic resistance, displayed modest killing by FZ88 [24]. This suggests that, as for other benzamides [17,21], the inactivity of these derivatives may be attributable to the action of efflux pumps or a membrane-permeability problem rather than to a lack of interaction with *E. coli* FtsZ. To date, there are no *in vitro* studies available evaluating the effects of these compounds on *E. coli* FtsZ that allow confirming or dismissing these hypotheses, and there are only a few *in vivo* studies.

In this work, we have analysed the impact of various 1,4-benzodioxane benzamides (Fig. 3) on the self-association of *E. coli* FtsZ *in vitro* in dilute solution, by reconstitution under conditions mimicking the crowded environment in the bacterial cytoplasm and *in vivo*. Besides a selection among the previously available 1,4-benzodioxane-benzamides, we have also tested in these assays newly synthesised hydroxylated derivatives of FZ88 (FZ112 and FZ113), to probe the effectiveness of this substitution on a compound with lower potency against Gram positives compared to FZ100, from which the above-mentioned hydroxylated compounds (FZ116 and FZ117) were derived. Using biochemical, biophysical, and imaging methods we have determined their effect on the depolymerisation kinetics, the GTPase activity and the size of the polymers formed by the protein. *In vivo* experiments have also been performed in parallel to evaluate which of the compounds are able to translate the *in vitro* effects to an antimicrobial activity, while taking into consideration their nature

as AcrAB efflux pump substrates. Our results demonstrate that many of the benzodioxane-benzamides tested significantly hyperstabilize *E. coli* FtsZ polymers *in vitro*, and these activities generally correlate with their ability to kill efflux-defective *E. coli* cells.

2. Results

2.1 Compounds design and preparation

Benzamide derivatives FZ14 – FZ100 were synthesized and purified as previously described [23,28–30]. In addition to the known derivatives and to obtain more polar analogues potentially able to cross the Gram-negative membrane, we started from the structures of FZ100 and FZ88, and we inserted an -OH group on the linker between the two main moieties, since we already observed that this portion is not directly implicated in the binding with *S. aureus* FtsZ [23,24,29]. Moreover, previous literature reports demonstrated how the introduction of hydroxy group in the linker position of other FtsZ benzamide inhibitors is slightly ameliorative rather than detrimental, for the antimicrobial activity towards Gram-positive strains [31]. For both FZ88 and FZ100, the introduction of a substituent in the above-mentioned position and the consecutive generation of a second stereogenic centre resulted in the need to isolate, characterize and test both the *erythro* and the *threo* diasteroisomers (Fig. 2).

The synthetic strategy to isolate compounds FZ112 and FZ113 (Scheme 1), derivatives of FZ88, resembles the one recently described by our research group [30] used to isolate FZ116 and FZ117, derivatives of FZ100. The synthesis started from catechol that underwent nucleophilic substitution with ethyl 2,3-dibromopropionate to achieve ring closure. Thus, the ester function was hydrolysed and soon converted to the corresponding methyl ketone, *via* Weinreb ketone synthesis, as previously described [32]. The α-bromination (intermediate 1) followed by the reduction of the ketone and the intramolecular elimination allowed the achievement of the corresponding epoxydic compound (intermediate 2), a key intermediate. Indeed, the rigidity of this moiety permitted the facile chromatographic separation of the two diastereoisomers. NMR literature data of the enantiopure *erythro* derivative [30] drove us toward the identification of the *erythro*, and, consequently, of the *threo*. Both *erythro* and *threo*, in parallel, subsequently underwent ring opening with the pharmacophoric benzamide, achieving the desired compounds FZ112 and FZ113. Similarly, this synthetic strategy was applied starting from 5,6,7,8-tetrahydronaphthalen-2,3-diol in place of catechol to obtain the final compounds FZ116 and FZ117 [30].

2.2 Benzodioxane-benzamides can delay disassembly of FtsZ polymers

Initial insight into the effects of the synthesised benzodioxane-benzamides on FtsZ polymerization was obtained from evaluation of the time-dependent disassembly of the one-subunit thick protofilaments the protein forms in dilute solution, using fluorescence anisotropy. Addition of GTP to FtsZ, with a tracer amount of FtsZ fluorescently labelled with Alexa 488, resulted in an increase of the anisotropy with respect to that of the unassembled protein, reflecting the formation of polymers, as previously described [34]. In the absence of the compounds and under our experimental conditions, anisotropy decreased over time upon GTP consumption, reaching basal levels in approximately 20 minutes after GTP addition (Fig. 4). In the presence of many of the benzodioxane-benzamides assayed, the FtsZ polymers disassembly was delayed to a higher or lower extent depending on the molecule (Fig. 4). In contrast, no substantial difference was found in the disassembly of FtsZ protofilaments upon addition of PC190723 at equivalent concentrations (Fig. 4a).

Simple substitution of the pyridothiazole moiety in PC190723 with 1,4-benzodioxane, leading to FZ14, did not have a significant impact on FtsZ disassembly, which was essentially insensitive to this compound (Fig.

4a). A moderate reduction of filament depolymerization was observed upon introduction of a methyl ester (FZ38), a 5-methylthio-1,2,4-oxadiazole (FZ82) or a 5-ethyl-1,2,4-oxadiazole (FZ90) at position 7- of the 1,4-benzodioxane ring (Fig. 4b and S1). The magnitude of the effect was similar for the methyl ester and the oxadiazoles. In contrast, FtsZ depolymerization was found to be virtually insensitive to compound FZ101, having a 5,6,7,8-tetrahydro-1,4-naphthodioxane moiety instead of the benzodioxane, and to FZ94, with a 1,4-naphthodioxane, at all concentrations evaluated (Fig. 4b and S1).

The introduction of a second carbon atom in the linker between the benzamide and the benzodioxane moieties of compound FZ14, giving rise to FZ88, also led to a moderate effect on FtsZ polymer lifetime (Fig. 4c and S1), comparable to that observed for derivatives FZ38, FZ82 and FZ90, that have additional substituents at position 7- but a single carbon in the linker. Interestingly, derivatives FZ95 and FZ100, in which the benzodioxane ring of FZ88 was replaced by a naphthodioxane or a 5,6,7,8-tetrahydro-1,4-naphthodioxane, respectively, highly stabilized the FtsZ protofilaments, impeding their depolymerization for long time periods (Fig. 4c and S1). Thus, at the lowest concentration assayed, FtsZ polymer disassembly took around 3-fold longer in the presence of FZ95 or FZ100 than in the absence of ligands (Fig. S1) and, at higher concentrations, filaments remained mostly assembled during the 60-minute observation window (Fig. 4c and S1). The time-dependent decrease in anisotropy (Fig. S1) indicated that the polymers remained dynamic when modified by compounds FZ95 or FZ100, despite their slower disassembly.

Lastly, we evaluated the derivatives characterized by an additional hydroxy group in the linker between the two main moieties of FZ88 and FZ100. Hydroxylation of compound FZ100 rendered two different diastereoisomers, derivatives FZ116 (*Erythro*) and FZ117 (*Threo*), with markedly different impacts on FtsZ assembly (Fig. 4d). Whereas FZ116 still notably prolonged FtsZ polymer duration, FZ117 stabilized the protofilaments against depolymerization to a lower extent. Compounds FZ112 and FZ113, resulting from hydroxylation of FZ88, did not modify FtsZ disassembly (Fig. 4d), suggesting that this modification interfered with the modest effect of this compound.

These data show that, unlike the widely studied benzamide derivative PC190723, many of the benzodioxane benzamides we have tested have the ability to modulate the assembly properties of FtsZ single-stranded polymers, prolonging their lifetime. The extent of the effect was dependent on the structural elements present in each compound and, in one case, it was sensitive to their stereochemistry, with the *Erythro* hydroxylated derivative presenting a stronger effect than the corresponding *Threo*.

2.3 Benzodioxane-benzamides can reduce FtsZ GTPase activity

We next evaluated the effect of the benzodioxane-benzamides on the GTPase activity of FtsZ, which is crucial for its function, by determining the hydrolytic activity of the *E. coli* FtsZ one-subunit thick polymers with and without the compounds. Interestingly, the same inhibitors that displayed significant stabilization of FtsZ polymers by anisotropy (FZ95, FZ100, and its *Erythro* hydroxy derivative FZ116) also were the most effective at inhibiting GTP hydrolysis, with GTPase activities only ~5-15% of the levels of FtsZ without any compound added (Fig. 5a and S2). Intermediate effects, leading to GTPase activity values ranging from 50-80% of the initial GTPase activity, were obtained for other compounds (FZ38, FZ82, FZ88, FZ90 and the *threo* derivative FZ117; Fig. 5a, b and S2), in good agreement with their moderate effect on the lifetimes of the protein polymers. The GTPase activity values observed for compounds FZ94 and FZ101 were equal, within error, to those obtained in the absence of ligands (Fig. 5c), consistent with their negligible effects, on the time-dependent disassembly of the polymers. Minor to negligible effects were also observed for compounds FZ112 and FZ113, obtained by hydroxylation of the FZ88, in line with their lack of effects on filament disassembly (Fig. 5c and S2).

These experiments show that some benzodioxane-benzamides can substantially reduce the GTPase activity of FtsZ and that there is a good correlation for the evaluated compounds between the level of reduction of the GTPase activity and the stabilization of the polymers against disassembly.

2.4 The effects of FZ95 and FZ100 benzodioxane-benzamides on FtsZ filaments are not associated with dramatic changes in their size

To better understand the effects of benzodioxane-benzamides on FtsZ, we evaluated their impact on the size distribution of the GTP-triggered protein polymers. For this purpose, we used a combination of analytical ultracentrifugation (sedimentation velocity, SV), fluorescence correlation spectroscopy (FCS) and dynamic light scattering (DLS) approaches, previously employed to characterize these polymers under different experimental conditions [35]. We focused here on FZ95 and FZ100, considering their large effect on the disassembly and GTPase activity of FtsZ. In the absence of the benzamide derivatives, FtsZ filaments displayed a sedimentation coefficient value around 14.5 S (Fig. 6a) and an apparent translational diffusion coefficient (D_{app}) value around 3.5-4 $\mu m^2/s$ (Fig. 6b, c), rendering a size around 80-100 subunits, in fair agreement with previous reports [36]. Addition of compounds FZ95 or FZ100 had a minor but detectable effect on both parameters, increasing the *s*-value of the polymers to around 16 S (Fig. 6a) and reducing the D_{app}-value of the assembled species to 3-3.5 $\mu m^2/s$ (Fig. 6b, c). This indicates that the number of subunits in the major polymeric species slightly increased in the presence of these compounds (around 100-140 *vs.* 80-100 subunits). No significant difference in the SV distribution was observed in the presence of compounds FZ94 or FZ101 compared to FtsZ filaments in their absence (Fig. S3), consistent with their negligible effects in the above-described anisotropy and GTPase activity assays.

To ascertain possible effects induced by the compounds on the morphology of the polymers, we turned to electron microscopy (EM). Images in the absence of the derivatives showed homogeneously distributed filaments with an average width of 5.5 ± 0.4 nm (Fig. 6d), typical for negative stained single-stranded FtsZ polymers [12]. In the presence of FZ95 or FZ100, no apparent changes were detected in the filaments, with average widths of 5.4 ± 0.5 nm or 5.3 ± 0.9 nm, respectively (Fig. 6d). Larger structures were sporadically observed in all the samples, whether containing the benzamide derivatives or not (Fig. S4).

2.5 Modulation of the effect of benzodioxane-benzamides under crowding conditions

To determine how the effects observed for the benzodioxane-benzamides on FtsZ assembly may be modulated by the crowded environment in the *E. coli* cytoplasm, the time-dependent depolymerization of FtsZ filaments was monitored in solutions containing dextran as a crowder, in the presence and absence of the compounds. In these crowding conditions, following GTP addition, *E. coli* FtsZ filaments completely depolymerized in around 50-60 minutes, at which time the anisotropy value reached the basal level (Fig. 7a). This time was longer than that observed in diluted solution, despite the lower amount of GTP (1 mM *vs.* 2 mM), because of the tendency of single stranded FtsZ polymers to form bundles in crowding conditions [15]. The modest increase in the net anisotropy values with respect to those in dilute solution (Fig. S1) is consistent with the formation of bundles and with the higher viscosity of the crowded solutions. In presence of compounds FZ95 and FZ100, the anisotropy value attained upon triggering polymerization with GTP remained stable for over 60 minutes (Fig. 7a). This result is compatible with a hyper-stabilizing effect on the FtsZ bundles mediated by the compounds (Fig. 7a, d), as previously observed for the single stranded protofilaments in dilute conditions. Parallel turbidity experiments with FtsZ in dextran with or without these compounds showed the same behaviour, with comparable depolymerization times (Fig. S5a).

Interestingly, compound FZ101, which had negligible effect on the stability of FtsZ polymers in dilute solution, significantly delayed disassembly of the bundles formed in dextran (Fig. 7b, d). FZ94 and the parent compound, FZ14, showed a subtle effect (*cf*. Fig. 7b, d and Fig. S5b). In striking contrast PC190723, also with no effect on the disassembly of FtsZ filaments in solution, accelerated disassembly of the filament bundles in dextran (*cf.* Fig. 4a and 7c). The strong stabilization of the bundles by FZ100 and FZ95, the moderate prolongation of their lifetime by FZ101 and even by FZ94 and the acceleration of disassembly by PC190723 were confirmed using Ficoll instead of dextran as crowding agent (Fig. S6).

The effect of FZ95 and FZ100 on FtsZ bundles formed in crowding conditions was also examined by confocal microscopy, which allowed visualization of these structures and monitoring of their disassembly with time. Confocal images obtained with FtsZ containing fluorescent FtsZ-Alexa 488 as tracer, in dextran, showed that addition of GTP triggered the formation of bundles, the morphology of which was not appreciably modified by the compounds (Fig. 7e). In accordance with the anisotropy data, the bundles completely disassembled 60 minutes after GTP addition due to exhaustion of the GTP by hydrolysis (Fig. 7e, top row) while, in contrast, they remained abundant in the presence of FZ95 or FZ100 (Fig. 7e, middle and bottom rows).

These experiments show that benzodioxane-benzamides inhibit disassembly of FtsZ filament bundles formed in crowding conditions that mimic the *E. coli* cytoplasm. This effect was observed for the ligands that largely enhance the lifetime of the single stranded polymers formed in dilute solution conditions, as well as for other compounds that have negligible effects on these non-bundled polymers. The opposite effect was found for PC190723.

2.6 Effects of the benzodioxane-benzamides on *E. coli* cell viability and division mostly correlate with their effects on FtsZ *in vitro*

To determine whether the *in vitro* effects of the compounds on FtsZ correlated with their effects on *E. coli* growth and division, we tested various compounds for their ability to inhibit the viability of *E. coli* mutants defective for efflux pumps. For MIC and cell filamentation assays, we used strain N43, which carries a mutation in the *acrA* gene (*acrA1*) encoding part of the efflux pump machinery. We first tested for minimum inhibitory concentrations (MIC) of the compounds on cells grown in liquid LB medium and found a wide range of effectiveness (Table 1). Consistent with their strong effects on FtsZ polymerization *in vitro*, the compounds with the most potency *in vivo* were FZ95 and FZ116, with MICs below 1 µg/ml. FZ88, FZ101 and FZ116's diastereoisomer FZ117 were next, with MICs of ~4 µg/ml (~10 µM), followed by FZ38, FZ82, and FZ90 (7.5-15 µg/ml, or ~18-38 µM). FZ112, FZ113 and FZ94 had little to no activity. Surprisingly, neither did FZ100 in the MIC assay, despite its strong effects *in vitro*.

We also measured cell filamentation of selected strains grown for the above assays. Such measurements of the ability of individual cells to divide are a more sensitive way to assay for cell division inhibition than the MIC assay, which merely measures culture turbidity, because non-dividing *E. coli* cells still increase in mass as they become long filaments. Consequently, a traditional MIC assay may underestimate the activity of a cell division inhibitor. We found that the MFC (minimum filamentation concentration) was often significantly lower than the MIC (Table 1). For example, the MFC for FZ95 was 0.24 µg/ml compared with its MIC, measured by loss of turbidity, of 0.94. Micrographs of cells treated with FZ95, FZ116, and FZ117 are shown in Fig. 8a. It is clear from the cell morphologies that very low concentrations of FZ95 or FZ116 strongly inhibit cell division and induce long filamentous cells, whereas similar concentrations of FZ117 do not. Despite the low sensitivity of the MIC turbidity assay compared with measuring filamentation microscopically, the trends remained the same, and reflected the *in vitro* activities.

2.7 Mutants in key cell division genes differentially affect susceptibility to the compounds in predictable patterns

We further investigated the effects of several of the compounds on various mutants of *E. coli* to determine whether changes in FtsZ or other cell division proteins could alter the susceptibility of the cells to the compounds. For this purpose we used a *ΔtolC::kan* allele, which inactivates the outer membrane portion of the efflux pump, to engineer several well characterized *E. coli* divisome mutant strains by phage P1 transduction. Once these *ΔtolC::kan* derivatives were constructed, we then tested them, along with the original N43 strain, by spotting serial dilutions of cells onto agar plates containing 6 μg/ml (~15 μM) of each compound. These spot viability assays are quantitative and potentially more sensitive than MIC assays, as they measure the ability of different quantities of cells to form individual colonies instead of turbidity of a population of cells in culture.

The results (Fig. 8b) show that the *ΔtolC::kan* parent strain (row 2) was unable to grow past 1-2 spots for all of the compounds tested. FZ100 (MIC >30 μg/ml) was actually quite effective at killing *ΔtolC* mutant *E. coli*, with a ~10^4-fold loss of plating efficiency (growth on the 1x and 10x dilutions only, with ~10^6 and 10^5 cells loaded on the 1x and 10x dilution spots, respectively, and no growth with 10^4 cells loaded). We also tested the N43 mutant of *E. coli* alongside the Δ*tolC* mutant as a control (row 6). Overall, N43 was equally or slightly less susceptible to the compounds compared with the Δ*tolC* strain, with the notable exception of FZ100, which was completely inactive on N43, consistent with the MIC assays. These results suggest that the N43 strain is specifically able to prevent FZ100 from entering cells (but not the other compounds tested) in a way that the Δ*tolC* strain is not.

We then asked whether gain of function variants of key cell division proteins could suppress the effects of the compounds. These variants, consisting of *ftsZ** (encoding $FtsZ_{L169R}$), *ftsA** ($FtsA_{R286W}$) and *ftsL** ($FtsL_{E88K}$), all at their native chromosomal locus, can suppress defects in cell division at stages after Z ring formation, such as inability to recruit and/or activate later division proteins. The latter two mutants in particular are hyperactive for cell division, forming smaller cells because they divide at shorter than normal cell lengths [37–39]. As a result, they are sometimes called “hyperfission” alleles. Purified FtsZ* protein forms double stranded polymers *in vitro* and has a strong tendency to form polymer bundles without the addition of crowding agents or other proteins [40]. The switch from a loose arrangement of FtsZ polymers to a more condensed arrangement is thought to be important for activation of septum synthesis [41], and the FtsZ* variant likely bypasses this switch.

We found that these three mutants conferred a consistent pattern of differential susceptibilities to classes of compounds. For example, the killing effect of FZ100 on the Δ*tolC* strain was completely suppressed by the *ftsA** allele (3rd row) but only weakly by the *ftsZ** allele (4th row). Notably, the other compounds with the strongest *in vitro* effects on FtsZ, FZ95 and FZ116, were also suppressed by the *ftsA** allele (although FZ95 was only partially suppressed). In striking contrast, the compounds with weaker *in vitro* effects on FtsZ polymerization in dilute solution, FZ38, FZ82, FZ90, FZ94, FZ101 and FZ117, showed the opposite pattern: they were only weakly suppressed by *ftsA** but strongly suppressed by *ftsZ** (compare rows 3 and 4). We conclude that the *ftsA** allele, despite affecting a different protein than the target, can better protect FtsZ from the strong polymer stabilizing compounds. This may be because *ftsA** promotes greater FtsZ turnover [42] compared with wild-type *ftsA*. Another possible explanation is that *ftsA** prematurely activates later steps of cell division [43], which might compensate for reduced FtsZ turnover mediated by FZ95, FZ100 and FZ116. FtsZ* also prematurely activates later steps of cell division, but likely through a distinct mechanism

[44]. It is not yet clear why compounds with weaker effects on dilute FtsZ compared with bundled FtsZ *in vitro* would be less effective on bundled FtsZ *in vivo*.

The effects of the *ftsL** hyperfission allele were more modest. FtsL protein normally activates the FtsWI septal peptidoglycan synthase complex in conjunction with its binding partner, FtsB, in response to signalling from other cell division proteins including FtsA [45]. However, the *ftsL** allele hyperactivates FtsWI by interacting directly with FtsWI in the periplasm [46]. We therefore predicted that *ftsL** might indirectly suppress the hyperstabilization of FtsZ polymers caused by some of the compounds by hyperactivating FtsWI.

We found that for most of the compounds with weaker *in vitro* activities, the *ftsL** allele had no suppressing effect (5th rows), probably because these compounds affect FtsZ in a way that cannot be compensated by a higher level of FtsWI activation. One such effect of these weaker compounds might be to prevent proper recruitment of FtsWI to the Z ring. However, the *ftsL** variant did have a modest suppressing effect on the compounds with the strongest *in vitro* activity, including FZ100 and FZ116 (5th rows). The suppression of FZ100 and FZ116, in particular, by *ftsA** and *ftsL** is consistent with the idea that these compounds hyperstabilize FtsZ polymers and this effect, which prevents FtsZ from functioning normally, can only be circumvented by compensatory hyperactivation of septum synthesis.

We then asked whether the well-known *ftsZ84* mutant, whose FtsZ (FtsZ$_{G105S}$) has lower GTPase activity than native FtsZ and which confers a thermosensitive division phenotype on *E. coli* cells, might suppress or exacerbate effects of the compounds. We again saw a pattern common to the compounds with the strongest *in vitro* effects on FtsZ: FZ100, FZ95, and FZ116. These compounds killed *ΔtolC ftsZ84* cells at the same efficiency as their Δ*tolC* parents, indicating that lower GTPase activity of the target did not affect the ability of these FtsZ hyperstabilizing compounds to inhibit cell division. In contrast, the *ftsZ84* allele was able to suppress the effects of compounds with weaker *in vitro* effects, including FZ38, FZ82, FZ90, FZ94, FZ101, and FZ117. This suppression was either a small 10-fold increase in viability (FZ101), a 100-fold increase (FZ38, FZ82, FZ90), or a greater than 1000-fold increase (FZ94, FZ117). These results suggest that the compounds with weaker effects *in vitro* require the GTPase activity of FtsZ to be effective, similar to other endogenous FtsZ inhibitors such as MinC [47]. On the other hand, the results indicate that compounds that hyperstabilize FtsZ polymers may act independently of their GTPase activity, perhaps because the G105S mutation and the compounds inhibit FtsZ dynamics through a similar mechanism.

Finally, we asked if making excess FtsZ could neutralize the effects of the compounds, which would provide strong evidence for FtsZ as their target, particularly in light of the recent report suggesting that *E. coli* FtsZ is not the target of PC190723 [20]. Toward this aim, we overexpressed FtsZ* instead of FtsZ to provide the best possible chance to neutralize the compounds. We found that cells with native FtsZ that also expressed uninduced levels of FtsZ* on a plasmid (pKG110-FtsZ*) were killed by 3 μg/ml of FZ95, FZ101 or FZ116 about as efficiently as cells with pKG110 empty vector (Fig. S7). However, when FtsZ* was overproduced from pKG110-FtsZ* by inducing cells with 1 μM sodium salicylate, complete viability was restored. The same was true when 6 μg/ml of the compounds were added. These results strongly suggest that the target of these compounds is FtsZ.

3. Discussion

In this work, we have found that some benzodioxane-benzamide FtsZ inhibitors initially designed to target *S. aureus* FtsZ optimally are also active on *E. coli* FtsZ at different organization levels, in dilute solution *in vitro*, in reconstituted systems resembling the crowded bacterial cytoplasm, and *in vivo*, on two *E. coli* strains defective in AcrAB-TolC efflux system.

Our results, summarized in Figure 9, indicate that some benzodioxane-benzamides can modulate the functional assembly properties of FtsZ, leading to hyperstabilization of FtsZ single-stranded protofilaments in dilute solution, with a concomitant decrease in GTPase activity. In contrast, the time-dependent disassembly of *E. coli* FtsZ polymers was insensitive to the reference molecule PC190723 under the dilute solution conditions used here. Replacement of the pyridothiazole moiety of PC190723 with 1,4-benzodioxane to obtain the parent compound FZ14 was not sufficient to induce significant activity. However, activity emerged with the addition of substituents at position 7- of the benzodioxane ring and by increasing the length of the carbon linker between the two rings. The largest effects in dilute solution were obtained for compounds FZ95, FZ100, and FZ116, all of which include the longer 2-carbon linker and a naphthodioxane or a 5,6,7,8-tetrahydro-1,4-naphthodioxane instead of the benzodioxane ring. The first two of these compounds also show high activity on *S. aureus* FtsZ, and indeed were designed for optimal binding to this protein through SAR analysis using a computational model [29]. Interestingly, FZ116, which is the *erythro* isomer of the hydroxylated derivative of FZ100, had activity similar to FZ100, whereas the *threo* isomer FZ117 had a significantly lower effect on FtsZ assembly and GTPase.

Stabilization of *E. coli* FtsZ filaments and reduced GTPase activity often correlate with increased lateral interactions and bundling of the protofilaments [12]. However, this does not seem to be the case here, as electron microscopy showed that the filaments remained single stranded in the presence of compounds, with an occasional small number of aggregates also found in their absence. Further analysis by orthogonal biophysical approaches showed a modest but reproducible increase in the average size of the polymers, reminiscent of the behaviour previously observed for FtsZ filaments induced by slowly hydrolysable analogues of GTP such as GMPCPP [36,48].

The marked prolongation of polymer lifetime by some of the compounds was also observed with polymer bundles formed under crowding conditions mimicking the intracellular environment. An interesting behaviour was found with FZ101 and perhaps also with FZ94, where the larger 5,6,7,8-tetrahydro-1,4-naphthodioxane moiety or a naphthodioxane replaced the benzodioxane ring in benzodioxane-benzamide structures containing only one carbon in the linker. With these compounds, the increased FtsZ protofilament duration and reduced GTPase activity, under the dilute solution conditions used here, were totally suppressed. Strikingly, in this case, the experiments in crowding conditions uncovered effects on the duration of the polymers not observed in dilute solution. This effect was clear for FZ101, and for FZ94 when Ficoll was used as a crowding agent, although there was only a small effect with dextran. This suggests that these molecules can influence lateral interactions between protofilaments within the bundles observed under these conditions. Another possibility is that small effects on the protofilaments, below the resolution of the techniques used, could be magnified in crowding conditions and hence detected. In any case, these results highlight the power of experimental approaches incorporating crowding, and other features of the natural environment in which targets exert their function, to understand the effects of drugs directed towards them [10]. Indeed, numerous studies have shown the profound impact of the overall high concentration of macromolecules inherent to all living systems on the reactions taking place in them, through excluded volume effects that favour large assemblies versus free species or compact versus extended conformations, as they exclude less volume compared with the other species [49,50]. One such example is the promotion of bundling of FtsZ protofilaments [15].

It is noteworthy that our *in vitro* data are generally well supported by *in vivo* activities of the various compounds. For example, FZ95 and FZ116, two of the three compounds with the strongest abilities to hyperstabilize FtsZ polymers *in vitro*, were also the most effective at inhibiting growth and division of efflux pump-defective *E. coli* cells. The third, FZ100, was much less effective *in vivo*, possibly because the higher

degree of ring saturation and the lack of a hydroxyl in the linker renders it less membrane permeable. Nevertheless, FZ100 shared with FZ95 and FZ116 a unique ability to be suppressed by the *ftsA** allele but less so by the *ftsZ** allele, indicating that all three of these compounds share a common mode of action despite the putative membrane permeability issues of FZ100. With one exception, the compounds with weaker *in vitro* activities were less able to inhibit *E. coli* growth and division and were rescued by the *ftsZ** allele but not the *ftsA** allele. This suggests that the higher oligomeric state of FtsZ has a role in interacting with these compounds. The exception, FZ101, shared the allele-specific pattern of the other weaker compounds but was a very potent inhibitor of *E. coli* viability. This might be explained by the ability of FZ101 to hyperstabilize FtsZ *in vitro* only when FtsZ polymers are in a bundled state, although it is not clear why the FtsZ* protein, expected to be in a bundled state *in vivo*, can neutralize the effects of FZ101 so efficiently. It should be emphasized, however, that when FtsZ* is overproduced, it completely neutralizes the effects of FZ95, FZ116 and FZ101, compounds with the strongest *in vivo* activities. This provides strong evidence that *E. coli* FtsZ is their direct target but indicates that further steps may be necessary to optimize these compounds to prevent resistant mutants from arising.

Our studies may also shed some light on the elusive mechanisms conferring the activity of the reference compound PC190723 on *E. coli*, for which *in vitro* and *in vivo* data have been controversial. We found that the FtsZ protofilament lifetime is insensitive to PC190723 in dilute solution, but FtsZ bundles formed in crowding conditions disassemble faster in its presence. This is in line with previous studies showing inhibition of FtsZ polymerization or bundling [21] or faster FtsZ disassembly [51]. The insensitivity of *E. coli* FtsZ to PC190723 found in other studies was initially attributed to the presence of a single residue (Arg or His) at position 307 and, more recently, to two salt bridges (Arg307/Glu198, Asp299/Arg202) and one hydrogen bond (OH group of Ser227 and the main chain of Gly191) blocking the interaction with the compound [22]. We speculate that perhaps certain interactions between FtsZ subunits within different protofilaments to form the crowding-induced bundles could interfere with the salt bridges or hydrogen bond that block the binding of PC190723, hence allowing the interaction. In any case, it seems that the mode of action of the benzodioxane-benzamides characterized here is very different from that of PC190723 when the target is *E. coli* FtsZ, since they stabilize the bundles rather than accelerate their disassembly.

4. Conclusions

The results presented in this work demonstrate how selected benzamides are able to interfere with *E. coli* FtsZ assembly. In particular, we observed how linear and lipophilic naphthodioxane moieties seem to be fundamental for disrupting essential FtsZ activities, such as dynamic polymer turnover and GTP hydrolysis. Furthermore, the length of the linker together with the presence of an attached hydroxylic pendant strongly contributes to these disruptive effects. Lastly, the stereochemistry of such derivatives plays a key role in the interaction with FtsZ, and specifically the *erythro* diastereoisomer seems to be preferred.

Benzamide derivatives have mostly been considered active only on Gram-positive bacteria. The demonstration that some of them can bind to *E. coli* FtsZ and perturb its critical properties should pave the way to using these compounds against Gram-negative bacteria, for which the number of identified active compounds is substantially lower.

5. Materials and methods

5.1 Chemistry

Starting material and all reagents and solvents were purchased from several commercial suppliers (Merck, Fluorochem, and TCI) and used without further purifications. Silica gel matrix was used in TLC on aluminium foils (having fluorescent indicator 254 nm) and in flash chromatography (p.s. = 40 – 63 µm) on Puriflash XS 420 (Sepachrom Srl, Rho (MI), Italy) visualizing at 254 nm or at opportune wavelengths. Varian (Palo Alto, CA, USA) Mercury 300 NMR spectrometer/Oxford Narrow Bore superconducting magnet operating at 300 MHz was used for all ^{1}H-NMR spectra while ^{13}C-NMR spectra were acquired at 75 MHz. Signal multiplicity is reported with the following abbreviations: s = singlet, d = doublet, dd = doublet of doublets, t = triplet, q = quadruplet, dq = doublet of quadruplets, m = multiplet, bs = broad singlet. Final compounds were analysed by reverse-phase HPLC using a Waters XBridge C-18 column (5 µm, 4.6 mm × 150 mm) on an Elite LaChrom HPLC system with a diode array detector (Hitachi, San Jose, CA; USA). Mobile phase: A, H_2O; B, acetonitrile, isocratic, ratio A/B 60%/40% with 15 minutes run time and 1 mL/min flow rate. Their purity was quantified at peculiar λ max values, depending on the compound, and all resulted in >95%. The relative retention times are reported in each experimental section. Melting points were determined by DSC analysis using a DSC 1020 apparatus (TA Instruments, New Castle, DE, USA). The ^{1}H-NMR spectra, ^{13}C-NMR spectra and HPLC chromatograms of derivatives **FZ112** and **FZ113** are reported in the supplementary material.

5.2 Synthesis

2-Bromo-1-(1,4-benzodioxane-2-yl)-ethanone (1): Bromine (0.24 mL, 3.12 mmol) was added dropwise to a solution of 1-(1,4-Benzodioxane-2-yl)-ethanone (0.55 g, 3.12 mmol) in Diethyl Ether (5 mL) at -20 °C. The mixture was stirred at that temperature for 2 h, then washed with 10% aqueous $Na_2S_2O_5$ (10 mL), dried over Na_2SO_4, filtered and concentrated under vacuum to yield 0.8 g of **1** as a yellowish oil. Yield: quantitative. **^{1}H-NMR (300 MHz, $CDCl_3$, δ):** 7.05 (m, 1H), 6.92 (m, 3H), 4.90 (m, 1H), 4.39 (m, 2H), 4.33 (dd, *J* = 13.8, 1.3 Hz, 1H), 4.12 ppm (dd, *J* = 13.8, 1.3 Hz, 1H).

2-(oxyran-2-yl)-1,4-benzodioxane (2): $NaBH_4$ (0.14 g, 3.69 mmol) was added to a solution of **1** (1.9 g, 7.39 mmol) in Methanol (19 mL) at 0 °C. The reaction mixture was stirred at 0 °C for 0.5 hours, concentrated under vacuum, diluted with Tetrahydrofuran (THF, 20 mL) and added dropwise to a suspension of NaH (0.21 g, 8.87 mmol) in THF (10 mL) at 0°C under a nitrogen atmosphere. The reaction mixture was stirred at room temperature for 2 hours, then concentrated under vacuum, diluted with Ethyl Acetate (20 mL) and phosphate buffer (pH= 7). The organic phase was washed with 10 % aqueous NaCl, dried over Na_2SO_4, filtered and concentrated under vacuum to give a brown residue. Elution with 9/1 Cyclohexane/Ethyl acetate on silica gel gave 0.3 g of *Erythro*-**2** and 0.18 g of *Threo*-**2** as colourless oils. Yield (cumulative): 36 %. **^{1}H-NMR *Erythro* (300 MHz, $CDCl_3$, δ):** 6.87 (m, 4H), 4.34 (dd, *J* = 11.4, 2.4 Hz, 1H), 4.15 (dd, *J* = 11.4, 6.7 Hz, 1H), 3.96 (m, 1H), 3.14 (ddd, *J* = 6.2, 3.9, 2.5 Hz, 1H), 2.92 (dd, *J* = 5.0, 3.9 Hz, 1H), 2.81 ppm (dd, *J* = 5.0, 2.5 Hz, 1H). **^{1}H-NMR *Threo* (300 MHz, $CDCl_3$, δ):** 6.85 (m, 4H), 4.32 (dd, *J* = 9.1, 2.3 Hz, 1H), 4.10 (m, 2H), 3.22 (m, 1H), 2.85 ppm (m, 2H).

***Erythro* 3-(2-(1,4-Benzodioxane-2-yl)2-hydroxyethoxy)-2,6-difluorobenzamide (FZ112):** A solution of 3-Hydroxy-2,6-difluorobenzamide (0.18 g, 1.06 mmol) in *N*,*N*-Dimethylformamide (DMF, 3 mL) was added to a solution of *Erythro*-**2** (0.18 g, 1.01 mmol) and K_2CO_3 (0.15, 1.11 mmol) in DMF (2 mL) at RT. The reaction mixture was stirred at 70°C for 2 hours, then concentrated under vacuum, diluted with Ethyl Acetate (20 mL) washed with 10 % aqueous NaCl (5 x 10 mL), dried over Na_2SO_4, filtered and concentrated under vacuum to give a brown residue. Elution with 6/4 Cyclohexane/Ethyl acetate on silica gel and subsequent elution with

7/3 water/ACN on C18 gave 0.05 g of **FZ112** as a white solid. Yield: 14 %. M.p. 92.3 °C, Tr: 3.9 min, purity: 98.7 %. **^{1}H-NMR (300 MHz, d_6-DMSO, δ):** 8.10 (s, 1H), 7.82 (s, 1H), 7.25 (td, *J* = 9.3, 5.3 Hz, 1H), 7.05 (td, *J* = 9.0, 1.8 Hz, 1H), 6.83 (m, 4H), 5.72 (d, *J* = 5.8 Hz, 1H), 4.41 (dd, *J* = 10.9, 1.6 Hz, 1H), 4.24 (m, 2H), 4.14 (m, 2H), 3.97 ppm (m, 1H). **^{13}C-NMR (75 MHz, d_6-DMSO, δ):** 161.8, 152.3 (dd, *J* = 239.9, 6.7 Hz), 148.4 (dd, *J* = 246.7, 8.3 Hz), 143.7 (dd, *J* = 10.8, 3.0 Hz), 143.6, 143.2, 121.9, 121.7, 117.5, 117.4, 117.1 (dd, *J* = 25.0, 20.5 Hz), 116.0 (dd, *J* = 8.7, 1.0 Hz), 111.3 (dd, *J* = 22.9, 3.5 Hz), 73.3, 71.4, 68.0, 65.0 ppm.

Threo **3-(2-(1,4-Benzodioxane-2-yl)2-hydroxyethoxy)-2,6-difluorobenzamide (FZ113):** A solution of 3-Hydroxy-2,6-difluorobenzamide (0.18 g, 1.06 mmol) in DMF (3 mL) was added to a solution of *Threo*-**2** (0.18 g, 1.01 mmol) and K_2CO_3 (0.15, 1.11 mmol) in DMF (2 mL) at RT. The reaction mixture was stirred at 70 °C for 2 hours, then concentrated under vacuum, diluted with Ethyl Acetate (20 mL) washed with 10% aqueous NaCl (5 x 10 mL), dried over Na_2SO_4, filtered and concentrated under vacuum to give a brown residue. Elution with 6/4 Cyclohexane/Ethyl acetate on silica gel and subsequent elution with 7/3 water/ACN on C18 gave 0.15 g of **FZ113** as a white solid. Yield: 36 %. M.p. 117.4 °C, Tr: 3.6 min, purity: 97.5 % **^{1}H-NMR (300 MHz, d_6-DMSO, δ):** 8.10 (s, 1H), 7.82 (s, 1H), 7.28 (td, *J* = 9.0, 5.4 Hz, 1H), 7.06 (t, *J* = 8.9 Hz, 1H), 6.82 (m, 3H), 5.54 (d, *J* = 4.9 Hz, 1H), 4.41 (d, *J* = 11.2 Hz, 1H), 4.22 (m, 2H), 4.07 ppm (m, 3H). **^{13}C-NMR (75 MHz, d_6-DMSO, δ):** 161.7, 152.4 (dd, *J* = 239.9, 6.6 Hz), 148.4 (dd, *J* = 247.1, 8.4 Hz), 143.8, 143.6, 143.4 (dd, *J* = 9.5, 4.9 Hz), 121.7, 121.2, 117.6, 117.3, 117.1 (dd, *J* = 25.0, 20.4 Hz), 116.1 (dd, *J* = 11.0, 2.1 Hz), 111.4 (dd, *J* = 22.9, 3.7 Hz), 74.0, 70.7, 68.0, 65.5 ppm.

5.3 Materials and working conditions for *in vitro* assays

PC190723 was obtained from Calbiochem. GTP, salts, and buffer components of analytical grade were purchased from Sigma. Dextran 500 and Ficoll 70 (from Sigma and GE Healthcare, respectively) were dialyzed prior to their use in 50 mM Tris-HCl pH 7.5, 300 mM KCl, and their final concentrations were calculated through the determination of the refractive index of the solutions, using refractive index increments (dn/dc) of 0.142 ml/g [52] and 0.141 ml/g [53], respectively.

In the experiments, the desired final compound concentrations were obtained directly diluting a specific stock compound solution in DMSO, keeping a final DMSO concentration of 1-2% in the sample, as specified. FtsZ was dialyzed in 50 mM Tris-HCl pH 7.5, 300 mM KCl, 5 mM $MgCl_2$, which is the working buffer in which all experiments were conducted.

5.4 *E. coli* FtsZ protein purification and labelling

E. coli FtsZ was purified with a calcium precipitation method as described previously [54]. Briefly, *E. coli* BL21 cells transformed with plasmid pMFV56 were grown at 37°C in LB containing kanamycin. Expression was induced with isopropyl-1-thio-ß-D-galactopyranoside (IPTG), cells were harvested by centrifugation and the pellet resuspended. After cell lysis through sonication and removal of the insoluble fraction by centrifugation, the supernatant containing FtsZ was subjected to two calcium-induced precipitation cycles and subsequent ionic exchange chromatography. The protein was stored at -80°C. FtsZ was covalently labelled using Alexa Fluor 488 succinimidyl ester dye (ThermoFisher) as previously reported [34]. Fractions with labelled protein were pooled and stored at −80 °C until used. The degree of labelling, determined by UV-visible spectroscopy quantification, ranged between 0.3 and 0.8 moles of fluorophore per mole of protein.

5.5 Fluorescence anisotropy experiments

Anisotropy experiments were conducted in a Spark® Multimode microplate reader (Tecan) at 25 °C with 485 and 535 nm excitation and emission filters, respectively, using 384 or 96 black polystyrene (non-binding surface), flat bottom microplates (Corning), essentially as described [55]. To monitor the time-dependent FtsZ depolymerization, the anisotropy of the solution containing FtsZ-Alexa 488 (50 nM) as tracer and unlabeled FtsZ up to a total concentration of 10 µM, with or without 10 or 20 µM (3.8 µg/mL or 7.2 µg/mL, respectively, considering an average molecular weight of 380 g/mol) of the tested compound (final DMSO concentration, 2%) was recorded with time, after 2 mM GTP addition. When present, crowders (Ficoll or dextran) were at 150 g/l, and GTP concentration was 1 mM. Control experiments ruled out a contribution of DMSO to the observed effects both in diluted and crowded solutions (Fig. S8a and S9a). No changes in the total intensity measured were observed in the presence of the compounds. Slight differences in the net anisotropy value for different batches of labelled protein did not influence the observed effects of the compounds. Depolymerization profiles are reported either as these net anisotropy values or, for the sake of comparison among compounds, Δ anisotropy values in which the anisotropy reached after full disassembly was subtracted from the values recorded over the time course, as specified in the corresponding figure legends. When no full depolymerization was observed within the observation window, the value subtracted was that reached after disassembly by FtsZ without any compound. The effects were so strong in these cases that minor differences in the value subtracted did not affect the conclusions. The areas under the anisotropy traces were calculated by using trapezoids for integration, equivalent to estimations using SigmaPlot software, as a means to facilitate comparison between different compounds and/or conditions. Reported values, average of at least three independent measurements, were normalized with respect of those obtained for FtsZ in the absence of compounds, and the errors were calculated by error propagation from S.D. Additionally, the statistical significance of differences was analyzed using a one-way analysis of variance (ANOVA) test conducted with GraphPad Prism (v. 10.0.0) software. Consistent conclusions were reached with the two types of analysis (error propagation and ANOVA).

5.6 GTPase activity measurements

FtsZ GTPase activity was determined through quantification of inorganic phosphate (Pi) released over time, using BIOMOL® GREEN assay (Enzo Life Sciences). 1 mM GTP was added to 10 µM FtsZ in absence and in presence of 20 µM of each benzamide derivative (final DMSO concentration, 1%). Aliquots were extracted every 20 seconds and the absorbance at 620 nm measured using a Varioskan Flash plate reader (Thermo), after mixing with BIOMOL GREEN reagent. The concentration of released Pi was determined from a standard curve. Activity values were calculated from the slope of the straight lines of the released Pi/time graphs. Control measurements showed that the FtsZ GTPase activity remained unchanged in the presence of 1% DMSO (Fig. S8b). Differences in the GTPase activity of FtsZ from different purification batches in the absence of the compounds did not change the trends obtained in their presence. Reported values, averages from three replicates in most cases (and at least two replicates for all samples), were normalized with respect to the activity in the absence of any compound. Errors correspond to propagation from S.D. Additionally, the statistical significance of differences was analyzed using a one-way ANOVA test conducted with GraphPad Prism (v. 10.0.0) software. Consistent conclusions were reached with the two types of analysis (error propagation and ANOVA).

5.7 Turbidity measurements

The turbidity of samples containing 10 μM FtsZ with or without 20 μM of the tested compound (final DMSO concentration, 2%) with dextran 500 (150 g/l) was determined at room temperature using a Varioskan Flash plate reader (Thermo). To monitor the time dependent FtsZ depolymerization, the absorbance at 350 nm was measured every 5 min for 70 min upon 1 mM GTP addition. Four independent replicates were collected for each sample in most cases (at least two replicates for all samples). Controls ruled out an effect from DMSO (Fig. S9b).

5.8 Confocal microscopy

Images were obtained with a LEICA TCS SP5 inverted confocal microscope equipped with an HCX PL APO 63x oil immersion objective (N.A. 1.4, Leica). The excitation line was 488 (Ar laser) for FtsZ-Alexa 488. Samples containing a total 10 μM FtsZ (with 1 μM FtsZ-Alexa 488) and 150 g/l dextran 500, with or without 20 μM of the tested compound (final DMSO concentration, 2%), were visualized in silicon chambers glued to a coverslip. Controls discarded a contribution of DMSO to the observed effects (Fig. S9c). The polymerization of FtsZ was achieved by addition of 1 mM GTP directly over the mixture. Two independent replicates were collected for each sample. The samples were visualized immediately after GTP addition and mixing, with an estimated elapsed time <30s (t = 0), and 1 hour after GTP addition (t = 1 h). Images were prepared with ImageJ [56].

5.9 Analytical ultracentrifugation

To assess the effect of the compounds on FtsZ polymers triggered by GTP, sedimentation velocity experiments were performed at 30,000 rpm and 20°C in an XLI analytical ultracentrifuge (Beckman-Coulter Inc.) equipped with both Raleigh interference and UV-VIS detection systems, using an An-50Ti rotor and 12-mm double-sector centerpieces. Sedimentation coefficient profiles were obtained by least square boundary modelling of sedimentation velocity data using the c(s) method as implemented in SEDFIT (Peter Schuck 2000). Samples containing 10 μM FtsZ, 2 mM GTP and a GTP-regeneration system (RS, 2 units/ml acetate kinase and 15 mM acetyl phosphate [57]) to avoid GTP depletion during sufficient time to allow polymer characterization were assayed in the presence of 20 μM of the compounds (final DMSO concentration, 1%), and compared with the sedimentation behaviour of FtsZ polymers alone. Controls ruled out a contribution from the DMSO (Fig. S8c).

5.10 Fluorescence correlation spectroscopy

FCS experiments were conducted in a Microtime 200 (PicoQuant) time-resolved confocal fluorescence microscope equipped with a pulsed laser diode head (LDH-P-C-485) for excitation, essentially as described [55]. All samples contained 10 nM FtsZ-Alexa 488 as tracer and additional unlabelled FtsZ up to a total of 10 μM. Polymerization was triggered with 2 mM GTP, including the enzymatic GTP-regeneration system (see above). When present, the concentration of the compounds was 20 μM (final DMSO concentration, 2%). Six independent replicates of each sample were prepared, measured and analysed essentially as described [34,55,58]. Briefly, coverslips were treated by PEGylation to avoid nonspecific adsorption of the protein. Autocorrelation curves were analysed with FFS Data Processor software (version 2.4 extended, Scientific Software Technologies Center, Belarus [59]) with a model that includes a term for the triplet state dynamics [58]. Profiles obtained for FtsZ-GTP were analysed using a two-diffusing species model, the fastest one fixed

to the diffusion obtained for the protein in the absence of GTP (i.e. unassembled FtsZ; ~50 μm^2/s) and the slowest one assigned to the FtsZ polymers. Parallel analysis including a third term with a diffusion fixed to that of the free dye rendered negligible contribution for this component, and apparent diffusion coefficients (D_{app}) for the polymers equivalent to those obtained with the two-species model. A slight increase was observed in the fractional contribution of the assembled species to the FCS autocorrelation profiles in the presence of the compounds (0.6-0.7 *vs* ~0.5, in the absence of any ligand), perhaps related with a higher proportion of FtsZ assembled into large polymers although, despite of the low concentration of labelled protein, we cannot rule out a higher contribution arising from the formation of polymers with higher brightness. Controls discarded a contribution from the DMSO in which the compounds were dissolved (Fig. S8d).

5.11 Dynamic light scattering

DLS experiments were performed using a Protein Solutions DynaPro MS/X instrument as described [48]. Samples contained 10 μM FtsZ and, when present, 20 μM compound (final DMSO concentration, 2%). FtsZ polymerization was triggered with 2 mM GTP, including the enzymatic GTP-regeneration system as described above for the SV and FCS experiments. Profiles were recorded and exported with Dynamics V6 software and analyzed using user-written scripts and functions in MATLAB (version 7.10, MathWorks, Natick, MA) as described [48] to get the apparent translational diffusion coefficient. Data are the average of at least four independent experiments ± S.D. Controls discarded a contribution from DMSO (Fig. S8e).

5.12 Estimate of FtsZ polymers size from hydrodynamic measurements

The number of FtsZ monomers in the polymers, both in the absence and presence of compounds FZ95 or FZ100, was obtained from their apparent molar mass calculated via the Svedberg equation using the *s*-values obtained from the analysis of the SV profiles and the average of the D_{app}-values obtained by DLS and FCS, as previously described [48].

5.13 Electron Microscopy

Samples were imaged essentially as described [36], using a JEOL JEM-1230 microscope. Briefly, 10 μM FtsZ, with and without the compounds (20 μM, final DMSO concentration 2%), was incubated with 2 mM GTP for 1 min, added to a carbon-coated glow-discharged copper grid, negatively stained with uranyl acetate, and visualized. Controls ruled out a contribution from DMSO (Fig. S8f). Filament widths were measured using Image J and the plot profile plugin of straightened polymers. Average widths ± S.D. were calculated from 50 to 100 polymers measured for each sample.

5.14 Bacterial strain constructions

To construct the various Δ*tolC* derivatives used in this study, bacteriophage P1 lysates carrying the Δ*tolC::kan* allele were used to transduce WM6601 (WM1074 with *leuO*::Tn*10*), WM1125 (*ftsZ84*), WM1659 (*ftsA**), WM4915 (*ftsZ** with *leuO*::Tn*10*), and WM6600 (*ftsL** with *leuO*::Tn*10*) to kanamycin resistance. Transductants were then streak purified and saved as WM6922 (Δ*tolC*), WM5188 (*ftsZ84 ΔtolC*) WM6917 *(ΔtolC ftsA**), WM6920 *(ΔtolC ftsZ**), and WM6921 *(ΔtolC ftsL**), respectively, which were used for the spot viability assays along with the *acrA1* derivative WM6794 (N43). WM1074 is a *lac*- derivative of wild-type

MG1655 *E. coli* K-12. Plasmids pKG110 (vector) or pKG110-FtsZ* [40] were transformed into WM6794 and maintained in that strain by supplementing growth medium with 15 µg/ml chloramphenicol.

5.15 Microscopy and MIC determination

All compounds were diluted in DMSO to a final stock concentration of 30 mg/ml (~75-80 µM depending on the compound's molecular mass) and stored at 4˚C. For MIC measurements, each compound was diluted 1:500 (1 µl compound in 500 µl LB), mixed thoroughly, then 100 µl of this was added to the first well of a 96 well microplate. 50 µl of this mixture was then transferred to the second well that contained 50 µl of LB, mixed, and 50 µl of that added to the third well containing 50 µl LB, and so on. 50 µl of cells (1:300 diluted from mid-log cells grown in LB medium) were then added to each well, resulting in final compound concentrations of 30, 15, 7.5, 3.75, 1.87, 0.94, 0.47, and 0.24 µg/ml, respectively. The microplate was then incubated overnight at 30˚C with shaking, and turbidity in each well was measured with a Biotek microplate reader at an optical density of 600 nm. For determining MFC or cell morphology, (3 µl) were taken from the wells with turbidity, added to a glass slide, and covered with a 1.5 mm coverslip. Cells were imaged with DIC optics using an Olympus BX60 microscope outfitted with a 100X oil (N.A. 1.4) objective and a Hamamatsu Orca CMOS detector, and images were acquired with Olympus CellSens software.

5.16 Spot viability assays

Cells for each strain were grown to mid-exponential phase in LB, and serially diluted 10-fold in separate rows of a microtiter plate. LB plates containing 6 µg/ml (15-18 µM) of each compound were made by pouring 25 ml of molten LB agar (~55˚C) into a petri dish and adding 5 µl of each compound from a 30 mg/ml stock solution, followed by thoroughly mixing in the added compound with the micropipette tip. After the plates were completely set and dry, 5 µl of cells from each well were then spotted onto LB plates containing 6 µg/ml of the indicated compound using a multichannel pipettor. The spots were allowed to dry under a flame and incubated overnight at 30˚C prior to photographing.

Author Contributions

L.S.: Conceptualization, Investigation, Data curation, Validation, Formal Analysis, Visualization and Writing – original draft, review and editing. B.M.: Conceptualization, Data curation, Validation, Supervision and Writing — review and editing. M.S-S.: Validation, Formal analysis, Investigation, Data curation, Visualization and Writing – review and editing. C.A.: Investigation, Formal Analysis, Data curation, and Writing— review and editing. V.S.: Conceptualization, Supervision, Project Administration, Resources, Writing— review and editing. G.R.: Funding acquisition and Writing – review and editing. S.Z.: Conceptualization, Data curation, Funding acquisition, Project administration, Supervision, Validation and Writing— original draft, review and editing. E.V.: Funding acquisition, Supervision, Resources, Writing— review and editing. W.M.: Conceptualization, Data curation, Funding acquisition, Project administration, Validation and Writing – original draft, review and editing.

Acknowledgements

We thank the staff of CIB Margarita Salas Confocal Laser and Multidimensional Microscopy (M. T. Seisdedos, G. Elvira and M. D. Hernández-Fuentes), Molecular Interactions (J.R. Luque-Ortega and Ó. Nuero) and Electron Microscopy (R Núñez and JF Escolar) Facilities for excellent assistance in imaging and

ultracentrifugation experiments and the Technical Support Facility for invaluable input. We thank P. Jiménez-Carpio for technical support. We thank M. Hrast and I. Zdovc for donating the *E. coli N43* strain.

This work was supported by the Spanish Ministerio de Ciencia e Innovación (grant numbers 2023AEP105 and PID2019-104544GB-I00/AEI/10.13039/501100011033, to G.R. and S.Z.). M.S.S. was supported by the Agencia Estatal de Investigación and the European Social Fund (grant number PTA2020-018219-I/AEI/10.13039/501100011033). W.M. was supported by the National Institutes of Health, USA (Grant number AI171856). The Systems Biochemistry of Bacterial Division group (CIB Margarita Salas) participates in the CSIC Conexiones LifeHUB (grant number PIE-202120E047). The funders had no role in study design, data collection and interpretation, or the decision to submit the work for publication.

References

[1] World Health Organization, Antibacterials in clinical and preclinical development: an overview and analysis. ISBN: 9789240047655, 2021. https://www.who.int/publications/i/item/9789240047655.

[2] WHO, WHO publishes list of bacteria for which new antibiotics are urgently needed, Geneva, 2017.

[3] A. Casiraghi, L. Suigo, E. Valoti, V. Straniero, Targeting Bacterial Cell Division: A Binding Site-Centered Approach to the Most Promising Inhibitors of the Essential Protein FtsZ, Antibiotics (Basel) 9 (2020) 1–28. https://doi.org/10.3390/antibiotics9020069.

[4] D.P. Haeusser, W. Margolin, Splitsville: structural and functional insights into the dynamic bacterial Z ring, Nat. Rev. Microbiol. 14 (2016) 305–319. https://doi.org/10.1038/nrmicro.2016.26.

[5] M. Vicente, A.I. Rico, The order of the ring: assembly of Escherichia coli cell division components, Mol. Microbiol. 61 (2006) 5–8. https://doi.org/10.1111/j.1365-2958.2006.05233.x.

[6] A. Typas, M. Banzhaf, C.A. Gross, W. Vollmer, From the regulation of peptidoglycan synthesis to bacterial growth and morphology, Nat. Rev. Microbiol. 10 (2011) 123–136. https://doi.org/10.1038/nrmicro2677.

[7] P. Pradhan, W. Margolin, T.K. Beuria, Targeting the Achilles Heel of FtsZ: The Interdomain Cleft, Front. Microbiol. 12 (2021) 732796. https://doi.org/10.3389/fmicb.2021.732796.

[8] N. Silber, C.L. Matos de Opitz, C. Mayer, P. Sass, Cell division protein FtsZ: from structure and mechanism to antibiotic target, Future Microbiol. 15 (2020) 801–831. https://doi.org/10.2217/fmb-2019-0348.

[9] J.M. Andreu, S. Huecas, L. Araújo-Bazán, H. Vázquez-Villa, M. Martín-Fontecha, The Search for Antibacterial Inhibitors Targeting Cell Division Protein FtsZ at Its Nucleotide and Allosteric Binding Sites, Biomedicines 10 (2022) 1–18. https://doi.org/10.3390/biomedicines10081825.

[10] S. Zorrilla, B. Monterroso, M.-Á. Robles-Ramos, W. Margolin, G. Rivas, FtsZ Interactions and Biomolecular Condensates as Potential Targets for New Antibiotics, Antibiotics (Basel) 10 (2021) 1–21. https://doi.org/10.3390/antibiotics10030254.

[11] S. Du, J. Lutkenhaus, At the Heart of Bacterial Cytokinesis: The Z Ring, Trends Microbiol. 27 (2019) 781–791. https://doi.org/10.1016/j.tim.2019.04.011.

[12] H.P. Erickson, D.E. Anderson, M. Osawa, FtsZ in bacterial cytokinesis: cytoskeleton and force generator all in one, Microbiol. Mol. Biol. Rev. 74 (2010) 504–528. https://doi.org/10.1128/MMBR.00021-10.

[13] C. Ortiz, P. Natale, L. Cueto, M. Vicente, The keepers of the ring: regulators of FtsZ assembly, FEMS Microbiol. Rev. 40 (2016) 57–67. https://doi.org/10.1093/femsre/fuv040.

[14] G. Rivas, C. Alfonso, M. Jiménez, B. Monterroso, S. Zorrilla, Macromolecular interactions of the bacterial division FtsZ protein: from quantitative biochemistry and crowding to reconstructing minimal divisomes in the test tube, Biophys. Rev. 5 (2013) 63–77. https://doi.org/10.1007/s12551-013-0115-1.

[15] J.M. González, M. Jiménez, M. Vélez, J. Mingorance, J.M. Andreu, M. Vicente, G. Rivas, Essential cell division protein FtsZ assembles into one monomer-thick ribbons under conditions resembling the crowded intracellular environment, J. Biol. Chem. 278 (2003) 37664–37671. https://doi.org/10.1074/jbc.M305230200.

[16] M. Artola, L.B. Ruiz-Avila, A. Vergoñós, S. Huecas, L. Araujo-Bazán, M. Martín-Fontecha, H. Vázquez-Villa, C. Turrado, E. Ramírez-Aportela, A. Hoegl, M. Nodwell, I. Barasoain, P. Chacón, S.A. Sieber, J.M. Andreu, M.L. López-Rodríguez, Effective GTP-replacing FtsZ inhibitors and antibacterial mechanism of action, ACS Chem. Biol. 10 (2015) 834–843. https://doi.org/10.1021/cb500974d.

[17] J.D. Rosado-Lugo, Y. Sun, A. Banerjee, Y. Cao, P. Datta, Y. Zhang, Y. Yuan, A.K. Parhi, Evaluation of 2,6-difluoro-3-(oxazol-2-ylmethoxy)benzamide chemotypes as Gram-negative FtsZ inhibitors, J. Antibiot. (Tokyo) 75 (2022) 385–395. https://doi.org/10.1038/s41429-022-00531-9.

[18] D.J. Haydon, N.R. Stokes, R. Ure, G. Galbraith, J.M. Bennett, D.R. Brown, P.J. Baker, V.V. Barynin, D.W. Rice, S.E. Sedelnikova, J.R. Heal, J.M. Sheridan, S.T. Aiwale, P.K. Chauhan, A. Srivastava, A. Taneja, I.

Collins, J. Errington, L.G. Czaplewski, An inhibitor of FtsZ with potent and selective anti-staphylococcal activity, Science 321 (2008) 1673–1675. https://doi.org/10.1126/science.1159961.

[19] D.W. Adams, L.J. Wu, L.G. Czaplewski, J. Errington, Multiple effects of benzamide antibiotics on FtsZ function, Mol. Microbiol. 80 (2011) 68–84. https://doi.org/10.1111/j.1365-2958.2011.07559.x.

[20] S. Khare, J. Hsin, N.A. Sorto, G.M. Nepomuceno, J.T. Shaw, H. Shi, K.C. Huang, FtsZ-Independent Mechanism of Division Inhibition by the Small Molecule PC190723 in Escherichia coli, Adv. Biosyst. 3 (2019) e1900021. https://doi.org/10.1002/adbi.201900021.

[21] M. Kaul, Y. Zhang, A.K. Parhi, E.J. Lavoie, D.S. Pilch, Inhibition of RND-type efflux pumps confers the FtsZ-directed prodrug TXY436 with activity against Gram-negative bacteria, Biochem. Pharmacol. 89 (2014) 321–328. https://doi.org/10.1016/j.bcp.2014.03.002.

[22] A.K. Sharma, S.M. Poddar, J. Chakraborty, B.S. Nayak, S. Kalathil, N. Mitra, P. Gayathri, R. Srinivasan, A mechanism of salt bridge–mediated resistance to FtsZ inhibitor PC190723 revealed by a cell-based screen, MBoC 34 (2023) ar16. https://doi.org/10.1091/mbc.E22-12-0538.

[23] V. Straniero, V. Sebastián-Pérez, M. Hrast, C. Zanotto, A. Casiraghi, L. Suigo, I. Zdovc, A. Radaelli, C. de Giuli Morghen, E. Valoti, Benzodioxane-Benzamides as Antibacterial Agents: Computational and SAR Studies to Evaluate the Influence of the 7-Substitution in FtsZ Interaction, ChemMedChem 15 (2020) 195–209. https://doi.org/10.1002/cmdc.201900537.

[24] V. Straniero, L. Suigo, A. Casiraghi, V. Sebastián-Pérez, M. Hrast, C. Zanotto, I. Zdovc, C. de Giuli Morghen, A. Radaelli, E. Valoti, Benzamide Derivatives Targeting the Cell Division Protein FtsZ: Modifications of the Linker and the Benzodioxane Scaffold and Their Effects on Antimicrobial Activity, Antibiotics (Basel) 9 (2020) 1–22. https://doi.org/10.3390/antibiotics9040160.

[25] W.C. Chai, J.J. Whittall, Di Song, S.W. Polyak, A.D. Ogunniyi, Y. Wang, F. Bi, S. Ma, S.J. Semple, H. Venter, Antimicrobial Action and Reversal of Resistance in MRSA by Difluorobenzamide Derivatives Targeted at FtsZ, Antibiotics (Basel) 9 (2020) 1–22. https://doi.org/10.3390/antibiotics9120873.

[26] C. Bolchi, F. Bavo, R. Appiani, G. Roda, M. Pallavicini, 1,4-Benzodioxane, an evergreen, versatile scaffold in medicinal chemistry: A review of its recent applications in drug design, Eur. J. Med. Chem. 200 (2020) 112419. https://doi.org/10.1016/j.ejmech.2020.112419.

[27] G. Chiodini, M. Pallavicini, C. Zanotto, M. Bissa, A. Radaelli, V. Straniero, C. Bolchi, L. Fumagalli, P. Ruggeri, C. de Giuli Morghen, E. Valoti, Benzodioxane-benzamides as new bacterial cell division inhibitors, Eur. J. Med. Chem. 89 (2015) 252–265. https://doi.org/10.1016/j.ejmech.2014.09.100.

[28] V. Straniero, M. Pallavicini, G. Chiodini, C. Zanotto, L. Volontè, A. Radaelli, C. Bolchi, L. Fumagalli, M. Sanguinetti, G. Menchinelli, S. Delogu, B. Battah, C. de Giuli Morghen, E. Valoti, 3-(Benzodioxan-2-ylmethoxy)-2,6-difluorobenzamides bearing hydrophobic substituents at the 7-position of the benzodioxane nucleus potently inhibit methicillin-resistant Sa and Mtb cell division, Eur. J. Med. Chem. 120 (2016) 227–243. https://doi.org/10.1016/j.ejmech.2016.03.068.

[29] V. Straniero, V. Sebastián-Pérez, L. Suigo, W. Margolin, A. Casiraghi, M. Hrast, C. Zanotto, I. Zdovc, A. Radaelli, E. Valoti, Computational Design and Development of Benzodioxane-Benzamides as Potent Inhibitors of FtsZ by Exploring the Hydrophobic Subpocket, Antibiotics (Basel) 10 (2021) 1–19. https://doi.org/10.3390/antibiotics10040442.

[30] V. Straniero, L. Suigo, G. Lodigiani, E. Valoti, Obtainment of Threo and Erythro Isomers of the 6-Fluoro-3-(2,3,6,7,8,9-hexahydronaphtho[2,3-b][1,4]dioxin-2-yl)-2,3-dihydrobenzo[b][1,4]dioxine-5-carboxamide, Molbank 2023 (2023) M1559. https://doi.org/10.3390/M1559.

[31] N.R. Stokes, N. Baker, J.M. Bennett, J. Berry, I. Collins, L.G. Czaplewski, A. Logan, R. Macdonald, L. Macleod, H. Peasley, J.P. Mitchell, N. Nayal, A. Yadav, A. Srivastava, D.J. Haydon, An improved small-molecule inhibitor of FtsZ with superior in vitro potency, drug-like properties, and in vivo efficacy, Antimicrob. Agents Chemother. 57 (2013) 317–325. https://doi.org/10.1128/AAC.01580-12.

[32] V. Straniero, A. Casiraghi, L. Fumagalli, E. Valoti, How do reaction conditions affect the enantiopure synthesis of 2-substituted-1,4-benzodioxane derivatives?, Chirality 30 (2018) 943–950. https://doi.org/10.1002/chir.22968.
[33] R. D. Clark, L. J. Kurz, Synthesis of the Enantiomers of Erythro-2-oxiranyl-1,4-benzodioxan, HETEROCYCLES 23 (1985) 2005–2012. https://doi.org/10.3987/R-1985-08-2005.
[34] B. Reija, B. Monterroso, M. Jiménez, M. Vicente, G. Rivas, S. Zorrilla, Development of a homogeneous fluorescence anisotropy assay to monitor and measure FtsZ assembly in solution, Anal. Biochem. 418 (2011) 89–96. https://doi.org/10.1016/j.ab.2011.07.001.
[35] B. Monterroso, C. Alfonso, S. Zorrilla, G. Rivas, Combined analytical ultracentrifugation, light scattering and fluorescence spectroscopy studies on the functional associations of the bacterial division FtsZ protein, Methods 59 (2013) 349–362. https://doi.org/10.1016/j.ymeth.2012.12.014.
[36] R. Ahijado-Guzmán, C. Alfonso, B. Reija, E. Salvarelli, J. Mingorance, S. Zorrilla, B. Monterroso, G. Rivas, Control by potassium of the size distribution of Escherichia coli FtsZ polymers is independent of GTPase activity, J. Biol. Chem. 288 (2013) 27358–27365. https://doi.org/10.1074/jbc.M113.482943.
[37] B. Geissler, D. Shiomi, W. Margolin, The ftsA* gain-of-function allele of Escherichia coli and its effects on the stability and dynamics of the Z ring, Microbiology (Reading) 153 (2007) 814–825. https://doi.org/10.1099/mic.0.2006/001834-0.
[38] M.-J. Tsang, T.G. Bernhardt, A role for the FtsQLB complex in cytokinetic ring activation revealed by an ftsL allele that accelerates division, Mol. Microbiol. 95 (2015) 925–944. https://doi.org/10.1111/mmi.12905.
[39] B. Liu, L. Persons, L. Lee, P.A.J. de Boer, Roles for both FtsA and the FtsBLQ subcomplex in FtsN-stimulated cell constriction in Escherichia coli, Mol. Microbiol. 95 (2015) 945–970. https://doi.org/10.1111/mmi.12906.
[40] D.P. Haeusser, V.W. Rowlett, W. Margolin, A mutation in Escherichia coli ftsZ bypasses the requirement for the essential division gene zipA and confers resistance to FtsZ assembly inhibitors by stabilizing protofilament bundling, Mol. Microbiol. 97 (2015) 988–1005. https://doi.org/10.1111/mmi.13081.
[41] G.R. Squyres, M.J. Holmes, S.R. Barger, D.R. Pennycook, J. Ryan, V.T. Yan, E.C. Garner, Single-molecule imaging reveals that Z-ring condensation is essential for cell division in Bacillus subtilis, Nat. Microbiol. 6 (2021) 553–562. https://doi.org/10.1038/s41564-021-00878-z.
[42] P. Radler, N. Baranova, P. Caldas, C. Sommer, M. López-Pelegrín, D. Michalik, M. Loose, BioRxiv 1–49.
[43] S. Pichoff, S. Du, J. Lutkenhaus, Disruption of divisome assembly rescued by FtsN-FtsA interaction in Escherichia coli, Proc. Natl. Acad. Sci. U. S. A. 115 (2018) E6855-E6862. https://doi.org/10.1073/pnas.1806450115.
[44] M. Krupka, V.W. Rowlett, D. Morado, H. Vitrac, K. Schoenemann, J. Liu, W. Margolin, Escherichia coli FtsA forms lipid-bound minirings that antagonize lateral interactions between FtsZ protofilaments, Nat. Commun. 8 (2017) 15957. https://doi.org/10.1038/ncomms15957.
[45] K.-T. Park, S. Du, J. Lutkenhaus, Essential Role for FtsL in Activation of Septal Peptidoglycan Synthesis, mBio 11 (2020). https://doi.org/10.1128/mBio.03012-20.
[46] L. Käshammer, F. van den Ent, M. Jeffery, N.L. Jean, V.L. Hale, J. Löwe, BioRxiv 1–46.
[47] A. Dajkovic, G. Lan, S.X. Sun, D. Wirtz, J. Lutkenhaus, MinC spatially controls bacterial cytokinesis by antagonizing the scaffolding function of FtsZ, Curr. Biol. 18 (2008) 235–244. https://doi.org/10.1016/j.cub.2008.01.042.
[48] B. Monterroso, G. Rivas, A.P. Minton, An equilibrium model for the Mg(2+)-linked self-assembly of FtsZ in the presence of GTP or a GTP analogue, Biochemistry 51 (2012) 6108–6113. https://doi.org/10.1021/bi300891q.
[49] G. Rivas, A.P. Minton, Macromolecular Crowding In Vitro, In Vivo, and In Between, Trends Biochem. Sci. 41 (2016) 970–981. https://doi.org/10.1016/j.tibs.2016.08.013.

[50] A.P. Minton, The influence of macromolecular crowding and macromolecular confinement on biochemical reactions in physiological media, J. Biol. Chem. 276 (2001) 10577–10580. https://doi.org/10.1074/jbc.R100005200.

[51] J.M. Andreu, C. Schaffner-Barbero, S. Huecas, D. Alonso, M.L. Lopez-Rodriguez, L.B. Ruiz-Avila, R. Núñez-Ramírez, O. Llorca, A.J. Martín-Galiano, The antibacterial cell division inhibitor PC190723 is an FtsZ polymer-stabilizing agent that induces filament assembly and condensation, J. Biol. Chem. 285 (2010) 14239–14246. https://doi.org/10.1074/jbc.M109.094722.

[52] Y. Liu, R. Lipowsky, R. Dimova, Concentration dependence of the interfacial tension for aqueous two-phase polymer solutions of dextran and polyethylene glycol, Langmuir 28 (2012) 3831–3839. https://doi.org/10.1021/la204757z.

[53] A.A. Fodeke, A.P. Minton, Quantitative characterization of polymer-polymer, protein-protein, and polymer-protein interaction via tracer sedimentation equilibrium, J. Phys. Chem. B 114 (2010) 10876–10880. https://doi.org/10.1021/jp104342f.

[54] G. Rivas, A. López, J. Mingorance, M.J. Ferrándiz, S. Zorrilla, A.P. Minton, M. Vicente, J.M. Andreu, Magnesium-induced linear self-association of the FtsZ bacterial cell division protein monomer. The primary steps for FtsZ assembly, J. Biol. Chem. 275 (2000) 11740–11749. https://doi.org/10.1074/jbc.275.16.11740.

[55] B. Monterroso, M.Á. Robles-Ramos, M. Sobrinos-Sanguino, J.R. Luque-Ortega, C. Alfonso, W. Margolin, G. Rivas, S. Zorrilla, Bacterial division ring stabilizing ZapA versus destabilizing SlmA modulate FtsZ switching between biomolecular condensates and polymers, Open Biol. 13 (2023) 220324. https://doi.org/10.1098/rsob.220324.

[56] C.A. Schneider, W.S. Rasband, K.W. Eliceiri, NIH Image to ImageJ: 25 years of image analysis, Nat. Methods 9 (2012) 671–675. https://doi.org/10.1038/nmeth.2089.

[57] E. Small, S.G. Addinall, Dynamic FtsZ polymerization is sensitive to the GTP to GDP ratio and can be maintained at steady state using a GTP-regeneration system, Microbiology (Reading) 149 (2003) 2235–2242. https://doi.org/10.1099/mic.0.26126-0.

[58] V.M. Hernández-Rocamora, C. Alfonso, W. Margolin, S. Zorrilla, G. Rivas, Evidence That Bacteriophage λ Kil Peptide Inhibits Bacterial Cell Division by Disrupting FtsZ Protofilaments and Sequestering Protein Subunits, J. Biol. Chem. 290 (2015) 20325–20335. https://doi.org/10.1074/jbc.M115.653329.

[59] V.V. Skakun, M.A. Hink, A.V. Digris, R. Engel, E.G. Novikov, V.V. Apanasovich, A.J.W.G. Visser, Global analysis of fluorescence fluctuation data, Eur. Biophys. J. 34 (2005) 323–334. https://doi.org/10.1007/s00249-004-0453-9.

Tables

Compound	MIC (μg/ml)[1]	MFC (μg/ml)[2]
FZ38	7.5	ND
FZ82	7.5	ND
FZ88	3.75	ND
FZ90	15	ND
FZ94	>30	7.5
FZ95	0.94	0.24
FZ100	>30	ND
FZ101	3.75	ND
FZ112	>30	>15
FZ113	>30	30
FZ116	<0.47	0.24
FZ117	3.75	0.94

Table 1. Minimum concentrations of compounds needed to inhibit growth and division of *E. coli* N43 (WM6794). [1] Minimum concentration of compound to prevent turbidity after overnight incubation in LB broth at 30˚C. [2] Minimum concentration of compound that induces cell elongation after overnight incubation in LB broth at 30˚C. ND: not determined.

Figure captions

Fig. 1. Development of the benzodioxane-benzamide FtsZ inhibitors class: Starting from **FZ14,** the modifications regarded the 7-position (see References 23,24 and 27-29) and the linker (see References 23 and 24) between the benzamide and the benzodioxane moieties. For each modification, a few examples of all the obtained derivatives are shown.

Fig. 2. Structural modifications of FZ100 and FZ88, leading to FZ116, FZ117, FZ112 and FZ113.

Fig. 3. Derivatives used for the current study: Compounds **FZ38, FZ82**, **FZ90, FZ94 and FZ101** represent the best derivatives obtained during the investigation of the 7-position substituents. **FZ88** is the lead derivative of the 2 carbon atoms linker sub-class and **FZ95** and **FZ100** represent the latest and strongest compounds, designed using all the information gained during the Structure-Activity Relationship studies. Lastly, **FZ112**, **FZ113**, **FZ116** and **FZ117** are the corresponding hydroxylated derivatives, *erythro* and *threo*, of **FZ88** and **FZ100**, respectively. Considering the independent denomination of these compounds in each synthetic work, in the present work we decided to rename them as FZXX, for the sake of clarity, as illustrated in the table.

Scheme 1. Synthetic pathway for the obtainment of FZ112 and FZ113.

Fig. 4. Benzodioxane-benzamide derivatives can slow FtsZ polymer disassembly: Representative fluorescence anisotropy-based depolymerization profiles of FtsZ in the absence and presence of the compounds showing: (a) the lack of effect of **PC190723** and **FZ14**; (b) concentration-dependent stabilization against disassembly (by compounds **FZ38**, **FZ82**, and **FZ90**) or insensitivity (to **FZ101** and **FZ94**) with molecules modified in the 7-position; (c) large (**FZ95** and **FZ100**) or modest (**FZ88**) enhancement of the polymers lifetime by compounds with two carbon atoms in the linker; (d) dissimilar effects of diastereoisomers resulting from hydroxylation of **FZ100** (**FZ116** and **FZ117**) and insensitivity to hydroxylated ligands derived from **FZ88** (**FZ112** and **FZ113**), with profiles of the parent compounds as reference. The concentration of the compounds in the graphs on the left was 20 μM, except for **FZ14** that was tested at 40 μM. Fluorescence anisotropy was recorded immediately after addition of 2 mM GTP, and the value measured after GTP consumption was subtracted. To facilitate comparison, the calculated areas under the anisotropy curves, at the specified final concentrations of the compounds, are represented on the right (profiles at 10 and 20 μM can be found in Fig. S1). Areas are normalized to FtsZ values in the absence of any compound (depicted by a horizontal dashed line). Values are the average of three independent measurements. Errors were estimated by propagation from SD. The statistical significance of differences was analyzed using a one-way ANOVA test. For all figures: ****, $P \leq 0.0001$; ***, $P \leq 0.001$; **, $P \leq 0.01$; *, $P \leq 0.05$; n.s., not significant, $P > 0.05$. We note that, although labelled as n.s., the P-value for FZ82 and FZ88 at 20 μM was below 0.1 and very close to 0.05. The "§" symbol indicates areas obtained from curves in which depolymerization was not complete in the evaluation time. It should be noted that the areas and the statistical significances are underestimated in these cases. The total concentration of FtsZ was 10 μM, with 50 nM FtsZ-Alexa 488 as tracer, in working buffer.

Fig. 5. Benzodioxane-benzamide derivatives can decrease the FtsZ GTPase activity: GTPase activity of FtsZ in the presence of the compounds, showing (a) a notable reduction in the presence of **FZ95**, **FZ100** and **FZ116** and a modest effect of **FZ117**, (b) intermediate reduction by **FZ38**, **FZ82**, **FZ88** and **FZ90** and (c) negligible effects of, **FZ112**, **FZ113**, **FZ94** and **FZ101**, consistent with the trend observed in the anisotropy assays. Each compound was at 20 μM concentration. Graphs correspond to the GTPase activities obtained as specified in the Materials and Methods section from data in Fig. S2 and normalized with respect to that measured for FtsZ in the absence of any compound (depicted by a horizontal dashed line). Reported values, averages from 3 replicates in most cases (and at least 2 replicates for all samples), were normalized with respect to the

activity in the absence of any compound. Errors were estimated by propagation from SD. The statistical significance of differences was analyzed using a one-way ANOVA test. For all figures: ****, P ≤ 0.0001; *, P ≤ 0.05; n.s., not significant, P > 0.05. We note that, although labelled as n.s., the P-value for FZ117 was below 0.1. The concentrations of FtsZ and GTP were 10 μM and 1 mM, respectively, in working buffer.

Fig. 6. Benzodioxane-benzamide derivatives FZ95 and FZ100 slightly modify the size of FtsZ polymers: (a) SV interference distributions of FtsZ polymers with and without **FZ95** and **FZ100**, showing a shift to larger sedimentation values in the presence of the compounds. (b) Normalized FCS autocorrelation curves of FtsZ polymers without and with **FZ95** and **FZ100**, showing a shift to longer timescales in the presence of the compounds. The curve of unassembled FtsZ (*i.e.* in the absence of GTP-RS; FtsZ-GDP) is shown for comparison. Solid lines are the fits corresponding to the models indicated in Materials and Methods section. Data are the average of at least six independent experiments ± SD. All samples contained 10 nM FtsZ-Alexa 488. (c) Apparent translational diffusion coefficients of FtsZ polymers determined by DLS and FCS (corresponding to the slowest species). A slight decrease in the D_{app} was found in the presence of the compounds. Data are the average of at least four independent experiments ± SD. (d) Electron microscopy images of FtsZ polymers formed in the presence or absence of compounds **FZ95** and **FZ100**. In all cases, concentrations were 10 μM FtsZ, 20 μM compound and 2 mM GTP, with RS (a-c). All experiments were performed in working buffer.

Fig. 7. Benzodioxane-benzamide derivatives stabilize the FtsZ bundles formed in the presence of crowding agents against disassembly: Representative depolymerization profiles of FtsZ (50 nM FtsZ-Alexa 488) (a) in the absence and presence of the benzodioxane benzamide derivatives **FZ100** and **FZ95,** and (b) **FZ94** and **FZ101** in dextran as crowding agent, showing stabilization of the bundles against depolymerization. (c) Curves in the presence of **PC190723** show the opposite effect. Assays were monitored by fluorescence anisotropy right after addition of 1 mM GTP. (d) The areas under the anisotropy curves, normalized to that obtained in the absence of compound (depicted by a horizontal dashed line), are shown for comparison. Values are the average of two to four independent experiments and errors are calculated by propagation from S.D. The statistical significance of differences was analyzed using a one-way ANOVA test. For all figures: ***, P ≤ 0.001; *, P ≤ 0.05; n.s., not significant, P > 0.05. The "§" symbols indicate areas obtained from curves in which depolymerization was not complete in the evaluation time. It should be noted that the areas and the statistical significances are underestimated in these cases. (e) Representative confocal images of FtsZ bundles (with 1 μM FtsZ-Alexa 488 as tracer) in presence or in absence of **FZ95** or **FZ100**, observed over time, evidencing the presence of the polymers for longer times with the compounds. In all experiments, the total concentrations of FtsZ and of the compounds, when present, were 10 and 20 μM, respectively. All experiments were performed in working buffer with 150 g/l dextran.

Fig. 8. Effects of representative compounds on the viability and division of efflux-defective *E. coli* cells with altered cell division proteins: (a) *E. coli* N43 (WM6794) was grown shaking overnight in LB medium in the presence of several compounds at different concentrations in μg/ml, and representative fields of cells were imaged using differential interference contrast microscopy. Scale bar, 4 μm. (b) Ten-fold serial dilutions of exponentially-growing *E. coli* derivatives listed were spotted on LB agar plates containing 6 μg/ml of each compound, incubated overnight at 30˚C, then photographed. Strains used were WM5188 (*ftsZ84 ΔtolC*) WM6922 (Δ*tolC*), WM6917 *(ΔtolC ftsA**), WM6920 *(ΔtolC ftsZ**), WM6921 *(ΔtolC ftsL**) and WM6794 (N43, *acrA1*). The positive control plate with DMSO lacking the compounds, showing full growth, is framed in black.

Fig. 9. Benzodioxane-benzamide structural features for optimal inhibition of *E. coli* FtsZ: The -OH, 2 carbon atoms linker, the napthodioxane moiety and the *erythro* configuration seem to represent the main features for an optimal inhibition of *E. coli* FtsZ.

Illustrations

International Journal of Biological Macromolecules – Suigo, L. et al – Figure 1

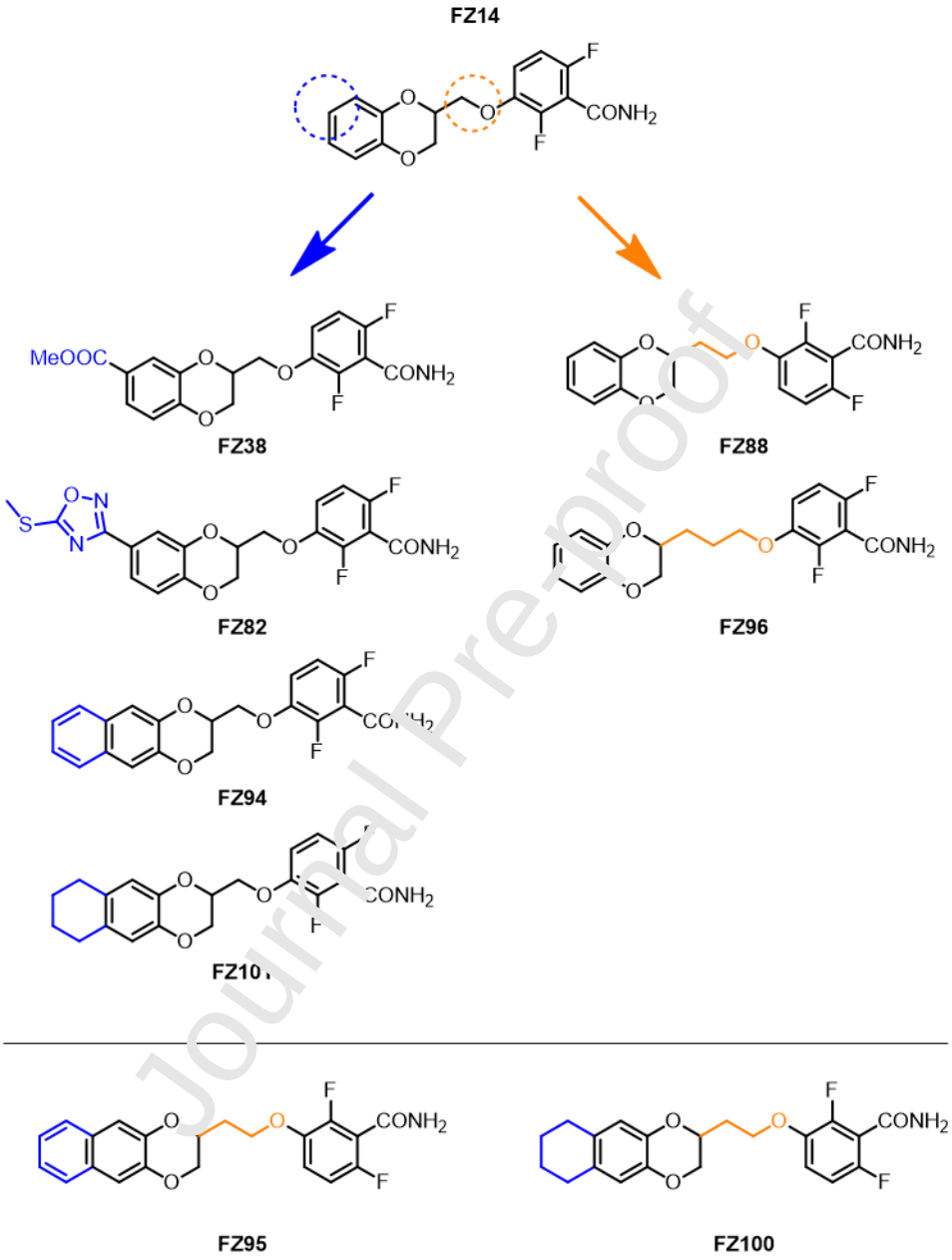

International Journal of Biological Macromolecules – Suigo, L. et al – Figure 2

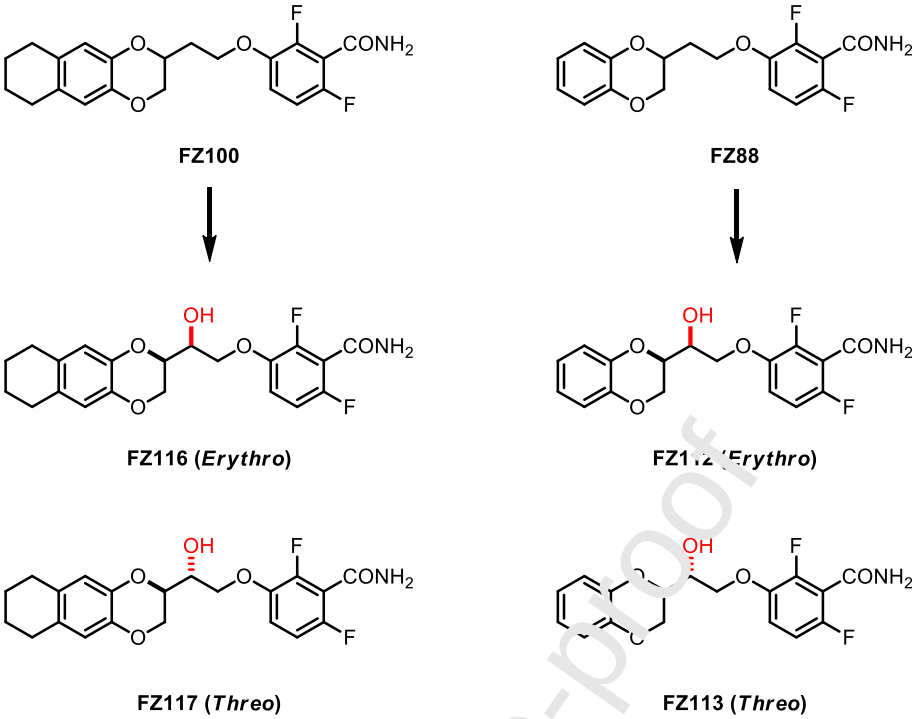

International Journal of Biological Macromolecules – Suigo, L. et al – Figure 3

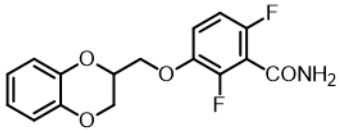

FZ14

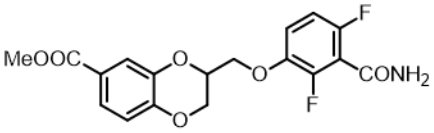

FZ38

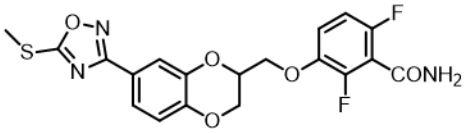

FZ82

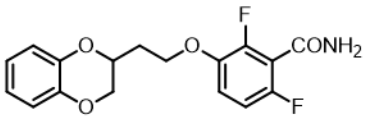

FZ88

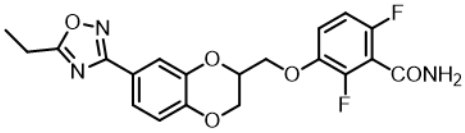

FZ90

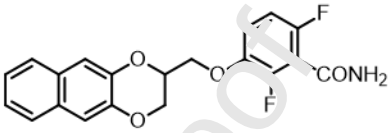

FZ94

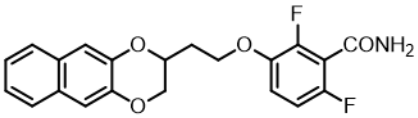

FZ95

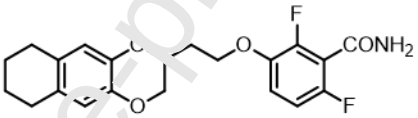

FZ100

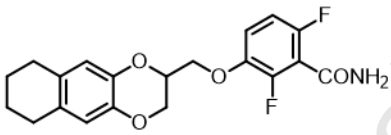

FZ101

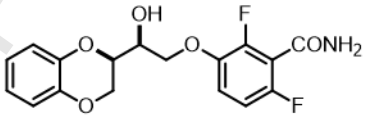

FZ112

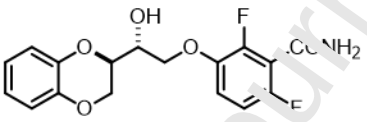

FZ113

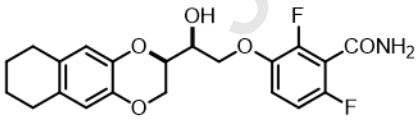

FZ116

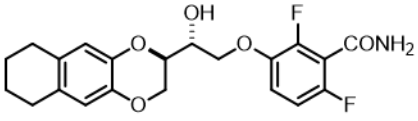

FZ117

Original denomination	Current denomination
11[a]	FZ14
21[b]	FZ38
9[c]	FZ82
7[d]	FZ88
11[c]	FZ90
4[e]	FZ94
5[e]	FZ95
8[e]	FZ100
7[e]	FZ101
1a *erythro*[f]	FZ116
1a *threo*[f]	FZ117

[a] [27] [b] [28] [c] [29] [d] [23] [e] [24] [f] [30]

International Journal of Biological Macromolecules – Suigo, L. et al – Scheme 1

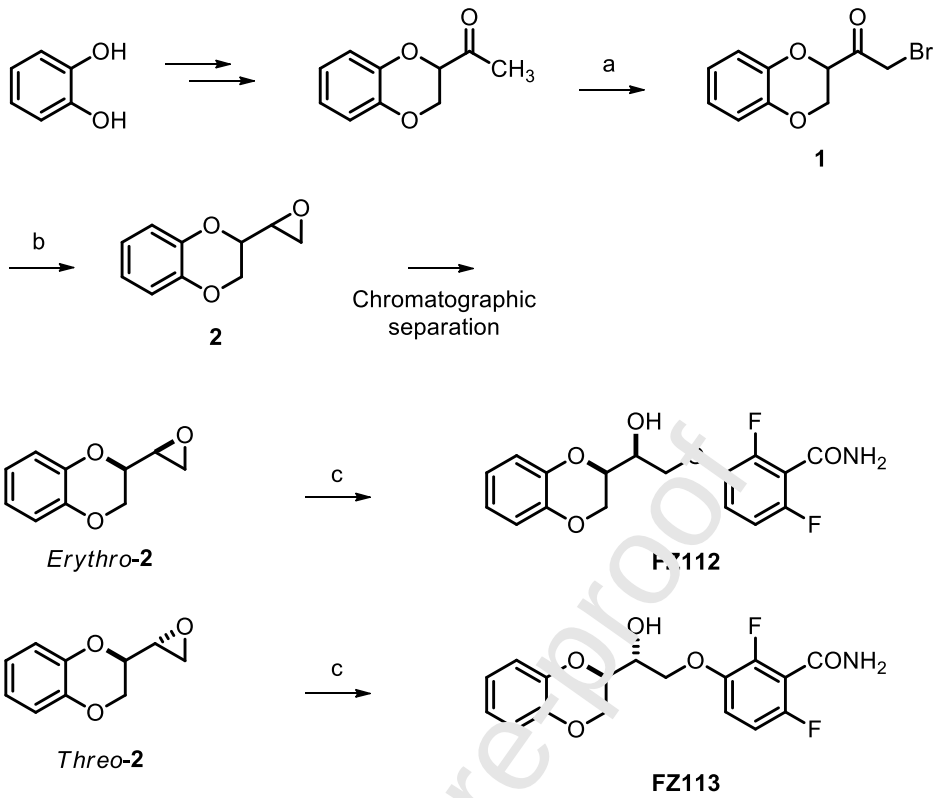

Reagents and conditions: a) Br_2, Et_2O, 0°C; b) 1. $NaBH_4$, MeOH, RT; 2- NaH, THF, RT; c) 2,6-difluoro-3-hydroxybenzamide, K_2CO_3, DMF, 70°C.

International Journal of Biological Macromolecules – Suigo, L. et al – Figure 4

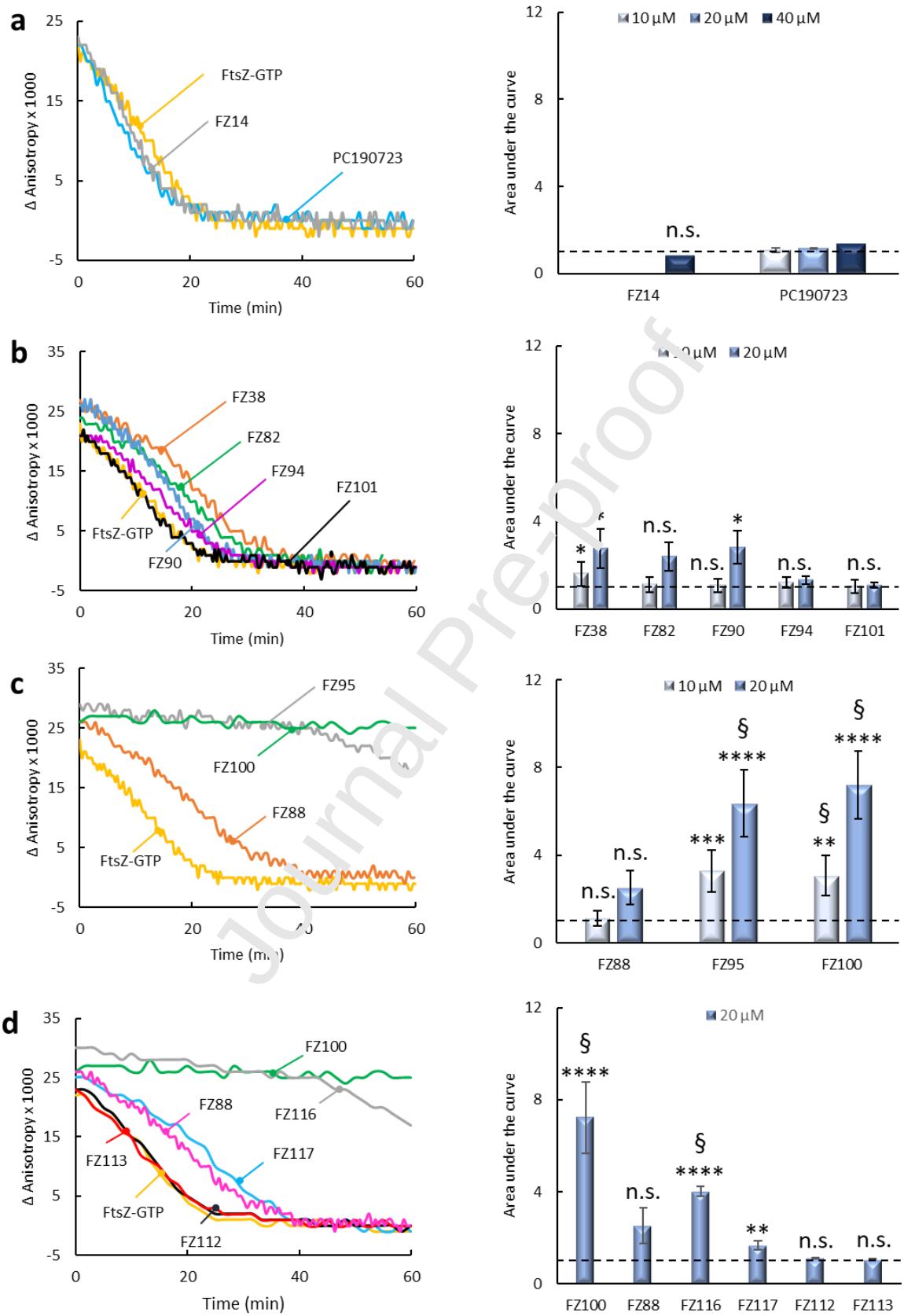

International Journal of Biological Macromolecules – Suigo, L. et al – Figure 5

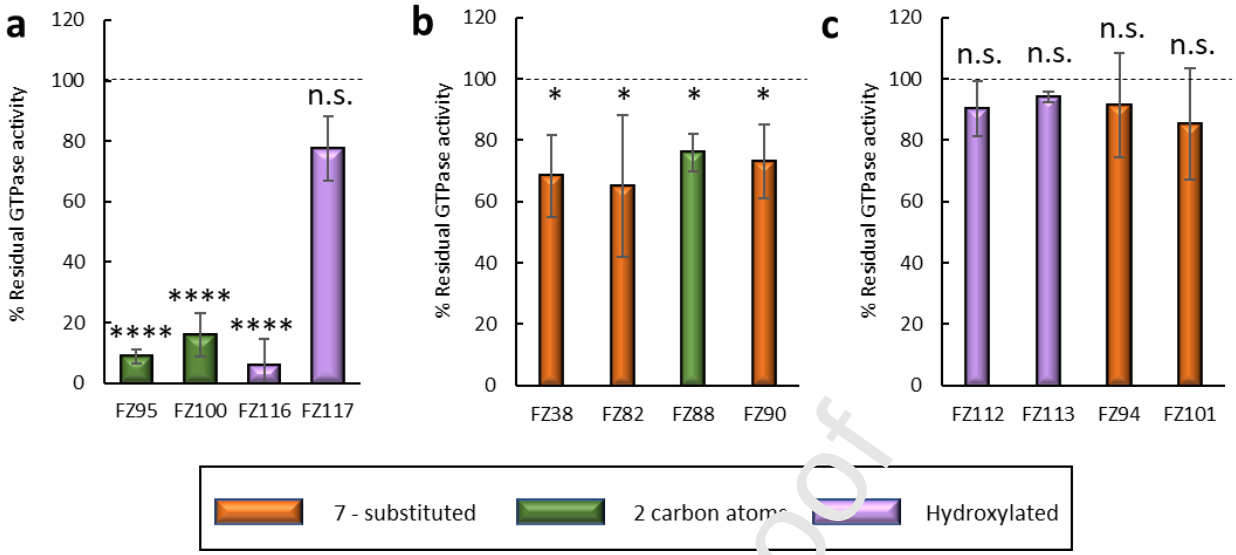

International Journal of Biological Macromolecules – Suigo, L. et al – Figure 6

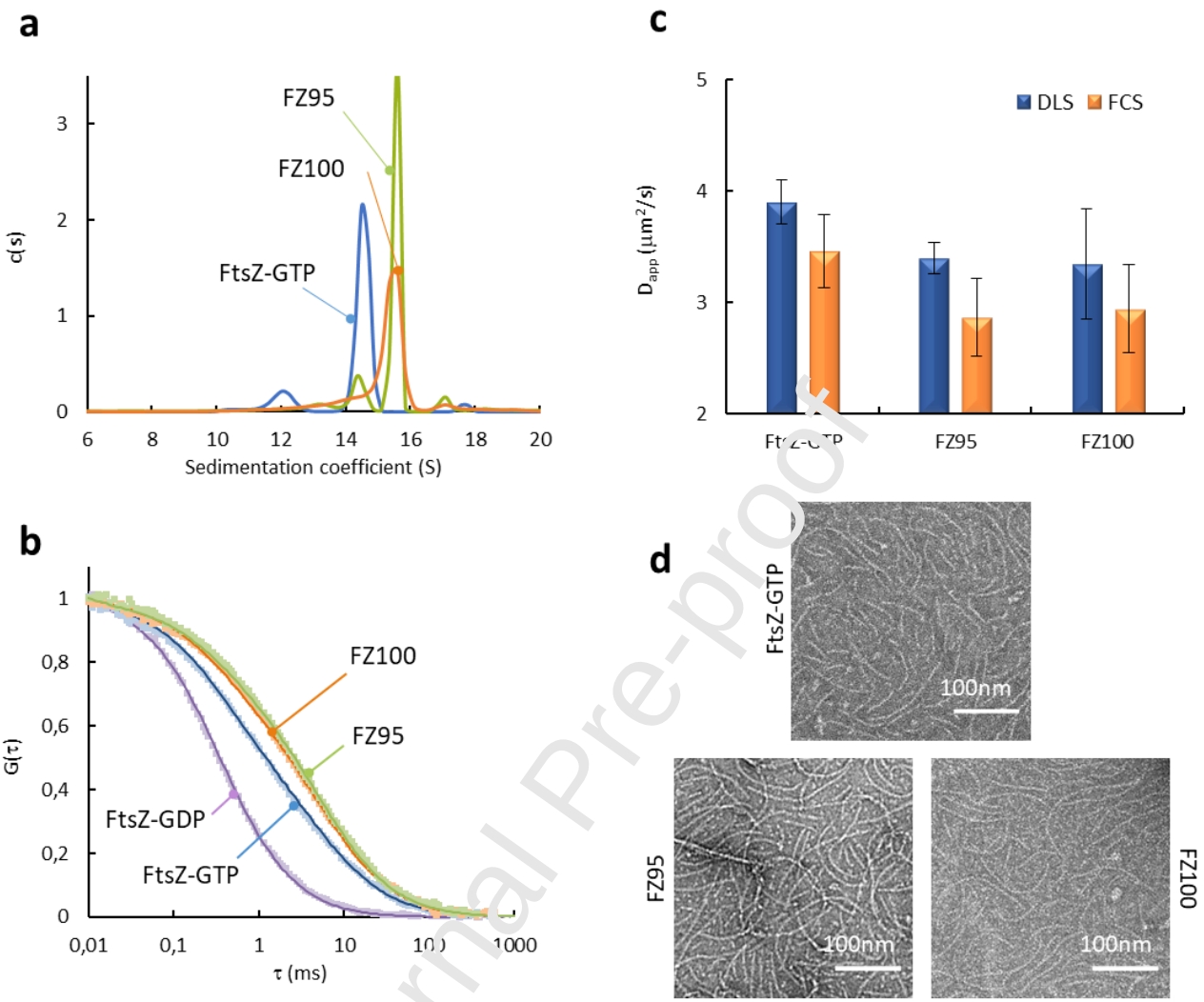

International Journal of Biological Macromolecules – Suigo, L. et al – Figure 7

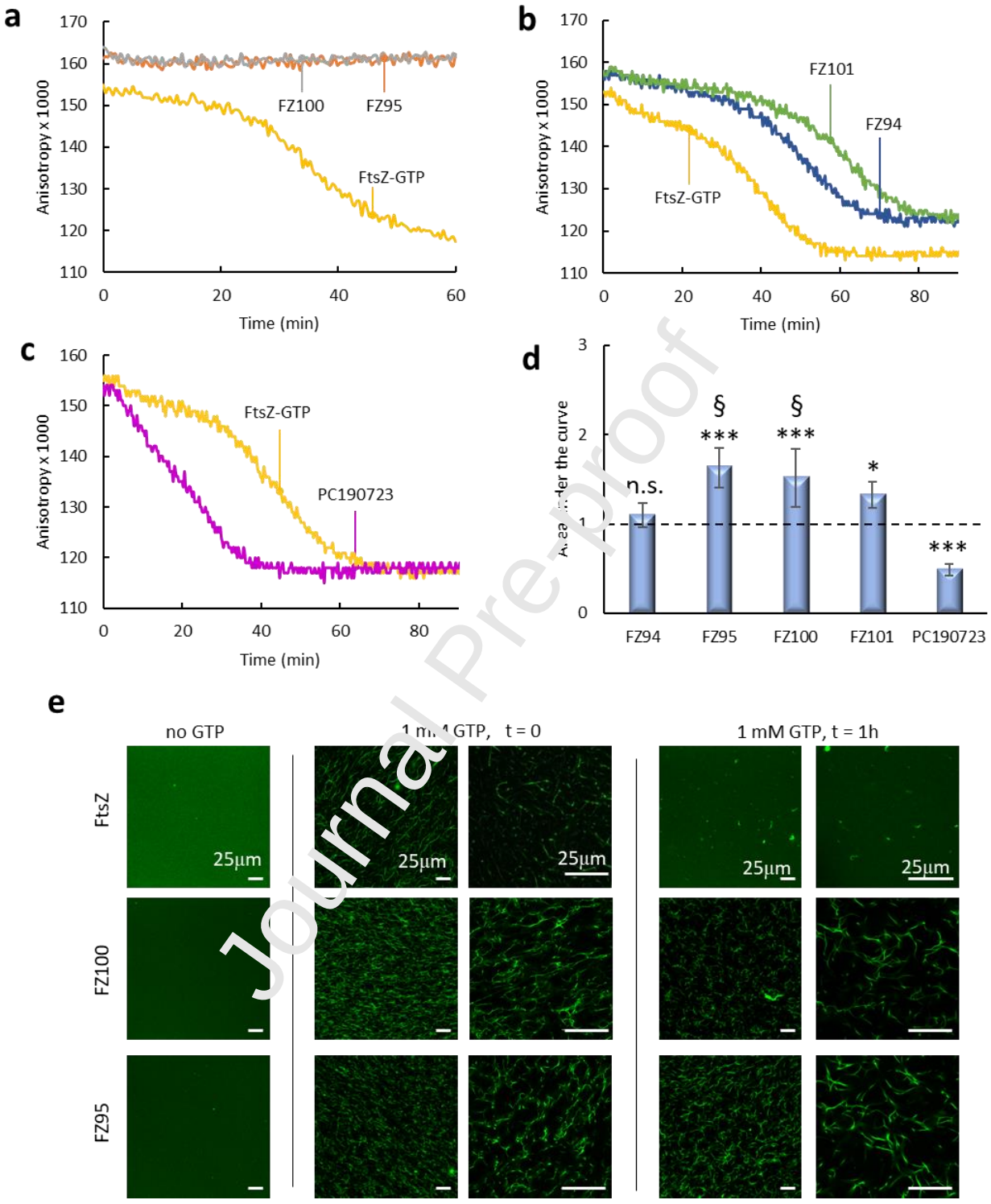

International Journal of Biological Macromolecules – Suigo, L. et al – Figure 8

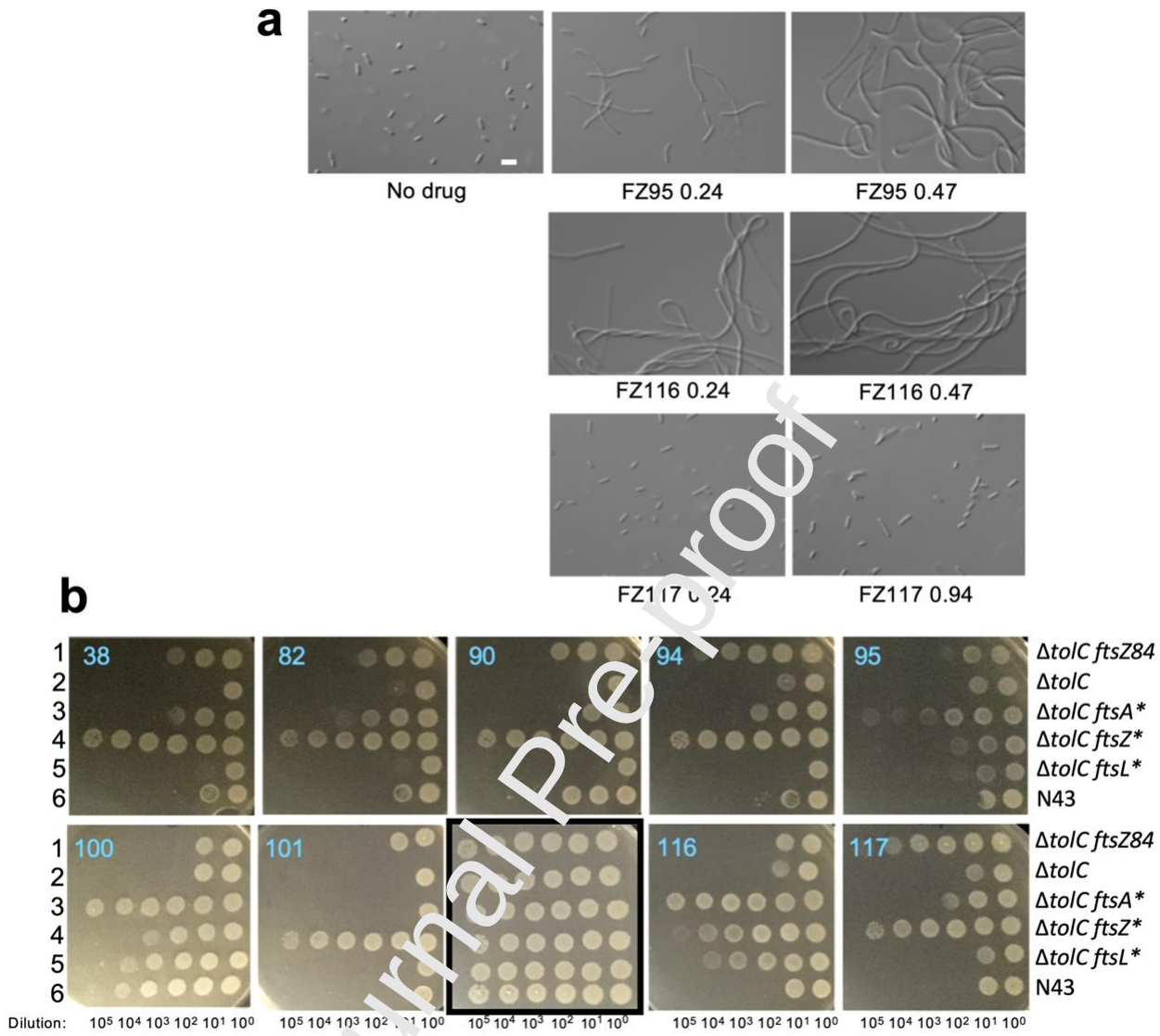

International Journal of Biological Macromolecules – Suigo, L. et al – Figure 9